Doctoral Dissertation

Studies on Selective Oxidation of Glycerol

Using Ceria-Zirconia Based Catalysts

(セリア–ジルコニア系触媒を用いた
グリセリンの選択的酸化に関する研究)

Yeon-Bin Choi

January 2022

Department of Applied Chemistry

Graduate School of Engineering

Osaka University

Preface

The study of this thesis has been conducted under the supervision of Professor Dr. Nobuhito Imanaka at Department of Applied Chemistry, Graduate School of Engineering, Osaka University.

The object of this thesis is to develop CeO_2–ZrO_2 based novel catalysts for the catalytic oxidation of glycerol under moderate condition.

The author wishes that the findings and the knowledge obtained in this work will provide useful suggestions and information for further development and design of novel catalysts for the conversion of glycerol into value-added compounds and that the materials would contribute to more practical applications.

Yeon-Bin Choi

Department of Applied Chemistry

Graduate School of Engineering

Osaka University

2-1 Yamadaoka, Suita,

Osaka 565-0871,

Japan

January, 2022

Contents

General Introduction

Biodiesel has been paid attention as a promising renewable fuel, produced from lipids; for instance; vegetable oils, animal oils, and waste fats. Biodiesel is generally produced by transesterification process of triglycerides and methanol, involved with the generation of glycerol as a byproduct. According to the Food and Agriculture Organization of United Nations (OECD/FAO) [1-4], the production of biodiesel is increasing year by year and it is forecasted to remain at a high level. Such an increase in the biodiesel production causes the oversupply and the devaluation of glycerol. Therefore, the utilization of the excess glycerol is an important issue.

The selective catalytic oxidation of glycerol has received significant attention because of its ability to transform glycerol into value-added compounds, such as glyceraldehyde (GLA), glyceric acid (GA), and hydroxypyruvic acid (HA) [4-6]. These compounds are important intermediates in chemical and medical industries. Based on the previous studies [1-7], the glycerol oxidation path are proposed as presented in Figure G-1. In the first step, the primary and secondary hydroxy group in glycerol are oxidized to generate GLA and DHA, respectively. When GLA is formed, it is easily oxidized to more chemically stable compound of GA. Further oxidation of GA results in C_2 compounds of glycolic acid (GLOA) and oxalic acid (OA). When DHA is generated,

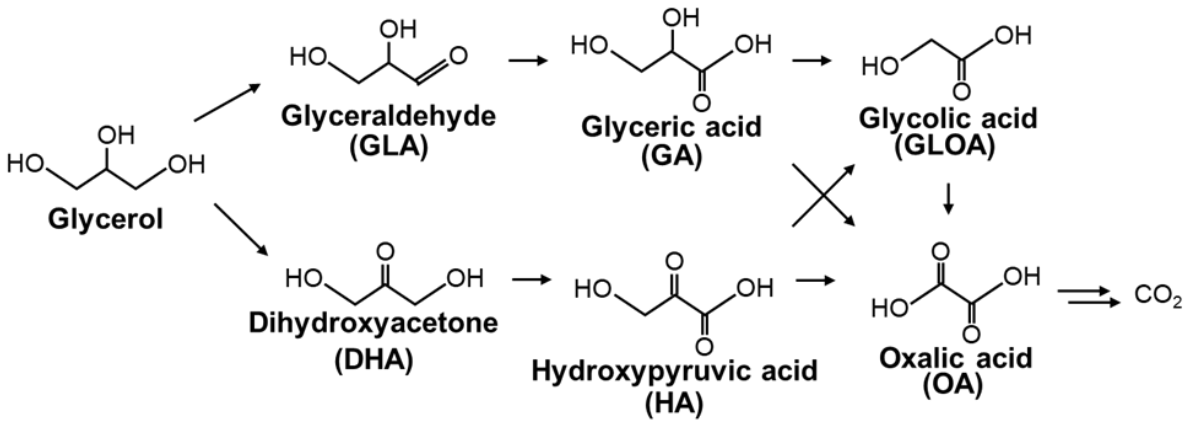

Figure G-1. Proposed reaction route from glycerol into value-added chemicals.

further oxidation of DHA generally yields the formation of GLOA and OA having high chemical stability via the intermediate of HA. Here, the final product is carbon dioxide.

For the selective glycerol oxidation, noble-metal (Pt, Pd, Au, etc.) based catalysts have been explicitly studied [7-9]. The selective oxidation ability is affected by pH value of reaction solution and nature of catalysts [8-9]. In base condition, catalysts generally lead to high product yields. **Table G-1** summarizes the reported catalytic activities for glycerol oxidation in base condition [9-11]. Au/graphite in the presence of NaOH under the pressure of 6 atm (O_2) is reported to show a high GA yield of 84% (estimated from the glycerol conversion (91%) and the GA selectivity (92%)) after the reaction for 3 h at 60°C [9]. In this catalyst, base condition is indispensable; that is, no activity was obtained in the base-free condition [9]. However, because they require a continuous supply of a base and an additional process is needed to obtain GA from sodium glycerate salt, the base-free synthesis route has received considerable attention.

Table G-2 shows the reported catalytic activities in base-free condition [12-22]. While the catalysts tend to show low activities compared to those in the base condition, several catalysts have relatively high activities. As an example, Pt/S-CNFs (S-CNFs: S-grafted carbon nanofibers) can convert glycerol to GA with high yield of 74.8% (estimated from the glycerol conversion (89.9%)

Table G-1. Summary of studies on catalytic glycerol oxidation in base condition

Catalyst	Glycerol conversion / %	Yield [a] / %	Reaction condition	Ref.
1% Au / graphite	91	84 (Y_{GA})	60°C, 6 atm (O_2), addition of NaOH	[9]
0.5% Au / graphite	75	26 (Y_{GA}), 22 (Y_{HA})	30°C, 3 atm (O_2), addition of NaOH	[10]
1% Pd / graphite	90	56.2 (Y_{GA})	30°C, 3 atm (O_2), addition of NaOH	[10]
5% Pd / carbon	90	70 (Y_{GA})	60°C, 0.75 mL·min^{-1} (air), addition of NaOH	[11]

[a] Y_{GA}: GA yield, Y_{HA}: HA yield

Table G-2. Summary of studies on catalytic glycerol oxidation in base-free condition

Catalyst [a]	Glycerol conversion / %	Yield [b] / %	Reaction condition	Ref.
Pt / S-CNFs	89.9	74.8 (Y_{GA})	60°C, 4 atm (O_2)+ 16 atm (N_2)	[12]
Pt-CeO_2 / carbon nanotubes	97.2	75.8 (Y_{GA})	60°C, 150 mL·min^{-1} (O_2)	[13]
1% Pt / carbon nanotubes	51.5	22.2 (Y_{GA})	60°C, 1 atm (O_2)	[14]
1% Pt / N-carbon nanotubes	76.1	42.3 (Y_{GA})	60°C, 1 atm (O_2)	[14]
5% Pt / carbon nanotubes	63.0	22.8 (Y_{GLA}), 23.6 (Y_{GA})	60°C, 150 mL·min^{-1} (O_2)	[15]
Pt / MCN	63.1	15.3 (Y_{GLA}), 40 (Y_{GA})	60°C, 3 atm (O_2)	[16]
5% Pt / carbon	90	55 (Y_{GA})	60°C, 0.75mL·min^{-1} (air)	[17]
Bi-Pt/ carbon	75.0	37 (Y_{DHA})	60°C, pH = 2, 1 atm (air)	[17]
5%Pt-5%Bi/ carbon	91.5	44.8 (Y_{DHA})	60°C, 150 mL·min^{-1} (O_2)	[18]
5%Pt-Cu / carbon	86.2	61 (Y_{GA})	60°C, 150 mL·min^{-1} (O_2)	[19]
PtCo / RGO	70.2	60.3 (Y_{GA})	60°C, 150 mL·min^{-1} (O_2)	[20]
Pt / K-AMC	67.6	53 (Y_{GA})	25°C, 10mL·min^{-1} (O_2)	[21]
5%Pt/S-MWNTs	90.4	61.7 (Y_{GA})	60°C, 150mL·min^{-1} (O_2)	[22]

[a] S-CNFs: S-grafted carbon nanofibers, MCN: mesoporous carbon nitride, RGO: reduced graphene oxide, K-AMC: KOH-activated mesoporous carbon, S-MWNTs: S-micropore free multiwall carbon nanotubes

[b] Y_{GLA}: GLA yield, Y_{GA}: GA yield, Y_{DHA}: DHA yield

and the GA selectivity (83.2%)) [12]. However, it requires the high pressure (4 atm O_2 and 16 atm N_2) and the heating at 60°C. Under the base-free and the atmospheric pressure conditions, it is recently reported that Pt-CeO_2/carbon nanotubes can produce GA from glycerol, that is the GA yield of 75.8% (estimated from the glycerol conversion (97.2%) and the GA selectivity (78%)) was

obtained [13]. However, it needs to heat at 60°C and to flow pure oxygen gas (150 mL·min^{-1}) to provide oxygen species to the catalyst. In the case of the air condition as well as the atmospheric pressure, only few studies were reported; e.g., Pt/C showed the high GA yield of 55% (glycerol conversion: 90%) in pH = 7 under the atmospheric pressure (air flow at 0.75 mL·min^{-1}) at 60°C [17]. For the production of intermediates of GLA, their reported yields were significantly lower than the case of GA having chemically stable; i.e., 22.8% of the GLA yield was reported using Pt/carbon nanotubes at 60°C under pure O_2 gas flow (150 mL·min^{-1}) [15] as listed in Table G-2. As for HA, the highest yield is still 22%, even in the base condition (Table G-1) [10].

The aim of this doctoral thesis is to realize the effective production of a desired product through the glycerol oxidation. To this end, one important issue is the moderate reaction conditions such as around room temperature in the atmospheric open-air system (1 atm) which enables the suppression of further oxidation. However, such moderate conditions generally cause a considerable decrease in the catalytic oxidation ability. Therefore, it is necessary to enhance the catalytic activity for the glycerol oxidation.

In order to improve the glycerol oxidation ability in the moderate reaction conditions (around room temperature, the atmospheric air), it is important to use promoters, which can supply an active oxygen species from inside the lattice toward activators. Schematic illustration of the role

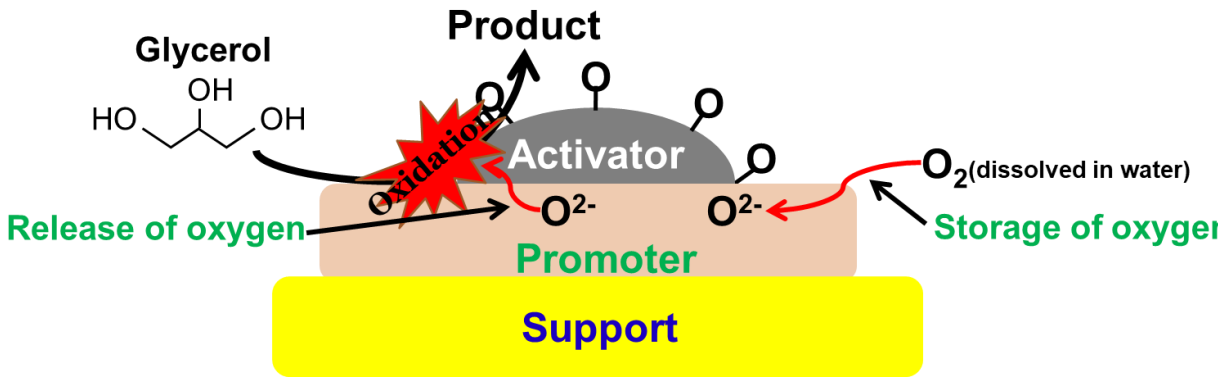

Figure G-2. Plausible process of oxygen supply on activator from promoter for the catalytic liquid-phase oxidation of glycerol.

of a promoter is drawn in **Figure G-2**. After glycerol is oxidized using the adsorbed oxygen on the activator, oxygen species should be released from the promoter lattice toward the activator for the continuous reaction. In order to compensate the lattice oxygen in the promoter, the oxygen molecule dissolved in the solution is stored as oxide ion. These processes of oxygen release and storage involve with the redox of the constituent cation in the promoter.

As a promoter, ceria-zirconia solid solution (CeO_2–ZrO_2) is well-known due to its oxygen release and storage abilities owing to the facile redox cycle of $Ce^{3+/4+}$ [23], and it has been already applied in automotive exhaust catalysts. However, CeO_2–ZrO_2 works at elevated temperatures over 800°C [24]. Therefore, it is necessary to improve the oxygen release and storage abilities of CeO_2–ZrO_2 to facilitate the oxidation ability of the supported activator even under moderate condition at around room temperature in the atmospheric air.

This thesis consists of the following three chapters.

Chapter 1 deals with the conversion of glycerol to GLA with high efficiency. In order to enhance the oxygen release and storage abilities of CeO_2–ZrO_2, the introduction of Fe_2O_3 into CeO_2–ZrO_2 was conducted for the improvement of the redox properties due to the $Fe^{2+/3+}$ valence change and the formation of the oxygen vacancies due to the low-valent $Fe^{2+/3+}$ substitution. In addition, mesoporous silica SBA-16 (Santa Barbara Amorphous No. 16) with high surface area was used as a support to increase the active sites. Thus, Pt/CeO_2–ZrO_2–Fe_2O_3/SBA-16 were prepared, and their catalytic activities for glycerol oxidation were investigated.

Chapter 2 aims to obtain GA by selective oxidation of glycerol. Since GA is obtained by the GLA oxidation, it is important to further improve the oxygen release and storage abilities. In addition, the lowering of acidity may be important to suppress the GLA desorption from active sites, because it is reported that high acidity caused the GLA desorption [2]. One simple and effective method is to increase the loading amount of CeO_2–ZrO_2–Fe_2O_3 in Pt/CeO_2–ZrO_2–Fe_2O_3/SBA-16. Therefore, the CeO_2–ZrO_2–Fe_2O_3 amount in Pt/CeO_2–ZrO_2–Fe_2O_3/SBA-16 was

increased, and their catalytic activities were investigated.

Chapter 3 deals with the production of HA from glycerol. The HA production requires the oxidation of both primary and secondary OH group in glycerol. Thus, Bi_2O_3 and PbO were introduced into CeO_2–ZrO_2, because the geometric effect among glycerol, Pt, and Bi^{3+} or $Pb^{2+/4+}$ may facilitate the secondary OH group in glycerol. Also, the low-valent Bi^{3+} and Pb^{2+} substitution and the redox of $Pb^{2+/4+}$ are expected to enhance the oxygen release and storage abilities. Therefore, Pt/CeO_2–ZrO_2–Bi_2O_3–PbO/SBA-16 catalysts were prepared, and their catalytic activities were investigated.

List of Publications

1. Glyceraldehyde Production from Glycerol over Pt/CeO_2-ZrO_2-Fe_2O_3/SBA-16 Catalysts Around Room Temperature in Open Air System

   Yeon-Bin Choi, Naoyoshi Nunotani, and Nobuhito Imanaka

   Materials Letters, 2020, *278*, 128392: 1-4.

2. Selective Glycerol Oxidation to Glyceric Acid under Mild Conditions Using Pt/CeO_2-ZrO_2-Fe_2O_3/SBA-16 Catalysts

   Yeon-Bin Choi, Naoyoshi Nunotani, Kunimitsu Morita, and Nobuhito Imanaka

   Journal of Asian Ceramic Societies, in press.

3. Production of Hydroxypyruvic Acid by Glycerol Oxidation over Pt/CeO_2-ZrO_2-Bi_2O_3-PbO/SBA-16 Catalysts

   Yeon-Bin Choi, Naoyoshi Nunotani, Kunimitsu Morita, and Nobuhito Imanaka

   Catalysts, 2022, *12*, 69: 1-8.

Supplementary publication

1. Selective Oxidation of Glycerol to Dihydroxyacetone Using CeO_2-ZrO_2-Bi_2O_3-SnO_2-Supported Platinum Catalysts

   Naoyoshi Nunotani, Masanari Takashima, Pil-Gyu Choi, **Yeon-Bin Choi**, and Nobuhito Imanaka

   Journal of Asian Ceramic Societies, 2020, *8*, 470-475.

Chapter 1

Novel catalysts for oxidation of glycerol to glyceraldehyde

1.1. Introduction

This Chapter deals with the effective production of GLA, generated by the oxidation of one primary OH group in glycerol. GLA is the simplest aldose with chemical formula $C_3H_6O_3$. Under prebiotic conditions using amino acid, GLA can be generated by coupling glycolaldehyde with formaldehyde, where D-GLA is predominantly formed when using L-glutamic acid [25,26]. GLA is an intermediate in the carbohydrate metabolism. GLA plays an important role in the pathogenesis of lifestyle-related diseases via the formation of GLA-derived AGEs (Advanced glycation end products) [27-29]. Here, glycation is the non-enzymatic reaction of sugar (glucose, etc.) and protein, also called the Maillard reaction [30], and AGEs are eventually generated through complex reactions. The AGEs generated through glycation are closely related not only to chronic diabetic complications such as glomerulosclerosis and renal arteriosclerosis [31-34] but also to neurodegenerative diseases such as Alzheimer disease [35], skin aging [36-38], and bone aging [39]. Therefore, GLA is used as the glycation inducer to assay AGEs formation *in vitro* [27]. In addition, GLA is one of the important chemicals for the application in medical and organic chemistry fields.

To date, it has been reported that the Pt/carbon nanotubes catalyst exhibited the high GLA yield of 22.8% (estimated from glycerol conversion (63.0%) and the GLA selectivity (36.2%)) [15]. However, it required the control of temperature at 60°C and the pure oxygen gas flow (150 $mL \cdot min^{-1}$), and such severe conditions facilitate further oxidation of GLA. In order to obtain the GLA product effectively, the moderate reaction condition and the high oxidation ability are required.

Here, it is important to introduce promoters which supply active oxygen species, as described in General Introduction section. Since commercial CeO_2-ZrO_2 needs elevated temperatures to work, Fe_2O_3 was introduced into the CeO_2-ZrO_2 lattice to improve the oxygen release and storage abilities, where the $Fe^{3+/2+}$ valence transition can lead to the improvement in the redox properties and the low-valent $Fe^{3+/2+}$ substitution may cause the smooth oxygen supply due to the formation of oxygen vacancies [40]. Because the surface area is also a key factor to increase the number of catalytic active sites, mesoporous silica SBA-16 (Santa Barbara Amorphous No. 16) having a large surface area and a felicitous pore size was selected as the catalyst support.

In this chapter, in order to realize the effective GLA production from glycerol under the moderate condition, the 7wt%Pt/16wt%$Ce_{0.8(1-x)}Zr_{0.2(1-x)}Fe_xO_{2-\delta}$/SBA-16 catalysts were prepared and investigated their catalytic abilities at 30°C under the atmospheric air pressure.

1.2. Experimental Procedure

Mesoporous silica SBA-16 (SBA) was prepared using a hydrothermal method according to the previous studies [41]. Pluronic F-127 (Sigma-Aldrich) (1.6 g), 1, 3, 5-trimethylbenzene (Kishida Chemical, ≥98.0%) (1.1 mL), and 90 mL of 0.2 $mol \cdot L^{-1}$ hydrochloric acid (prepared by diluting concentrated hydrochloric acid (Kishida Chemical, 35%) with deionized water) were mixed, and then 7.1 mL of tetraethoxysilane (Kishida Chemical, ≥99.0%) was added to the solution. After stirring at 35°C for 24 h, the mixture was hydrothermally heated at 140°C for 24 h in a sealed brass vessel using a Teflon bottle. The resulting precipitates were filtered by suction filtration, washed with water and ethanol, subsequently dried at 80°C for 12 h, and finally calcined at 600°C for 4 h under a flow of air (15 $mL \cdot min^{-1}$).

16wt%$Ce_{0.8(1-x)}Zr_{0.2(1-x)}Fe_xO_{2-\delta}$/SBA-16 (CZFe($x$)/SBA) samples were synthesized via a co-precipitation process. Aqueous solution of 1.0 mol·L^{-1} $Ce(NO_3)_3$, 0.10 mol·L^{-1} $ZrO(NO_3)_2$, and 0.10 mol·L^{-1} $Fe(NO_3)_3$ were prepared by dissolving $Ce(NO_3)_3·6H_2O$ (Kojundo, 99.9%), $ZrO(NO_3)_2·2H_2O$ (Kishida Chemical, ≥99.0%), and $Fe(NO_3)_3·9H_2O$ (FUJIFILM Wako Pure Chemical, 99.9%) in deionized water, respectively. The SBA-16 powder (0.4 g) was suspended into 1.0 mol·L^{-1} $Ce(NO_3)_3$ aq., 0.1 mol·L^{-1} $ZrO(NO_3)_2$ aq., and 0.1 mol·L^{-1} $Fe(NO_3)_3$ aq. in the stoichiometric ratio, and then, stirred for 30 min at room temperature. By dropwise addition of 5.0vol% NH_3 aqueous solution (prepared by diluting aqueous NH_3 (Kishida Chemical, 28%) with deionized water), the pH of the solution was adjusted to be 11 and further stirred at room temperature for 12 h. The precipitated product was collected by filtration, dried at 80°C, and then calcined at 900°C for 1 h.

Platinum was loaded onto $Ce_{0.8(1-x)}Zr_{0.2(1-x)}Fe_xO_{2-\delta}$/SBA-16 by mixing platinum colloid stabilized in polyvinylpyrrolidone (Pt-PVP, Pt: 4.0wt%, Tanaka Kikinzoku Kogyo) with $Ce_{0.8(1-x)}Zr_{0.2(1-x)}Fe_xO_{2-\delta}$/SBA-16 (0.4 g) in ethanol (40 mL). The loading amount of Pt was adjusted to be 7wt% by using 0.75 g of Pt-PVP, respectively. The mixture was stirred at room temperature for 6 h, followed by the evaporation of the solvent at 90°C. The residue was ground and then calcined at 500°C for 4 h in the atmospheric air to obtain the 7wt%Pt/16wt%$Ce_{0.8(1-x)}Zr_{0.2(1-x)}Fe_xO_{2-\delta}$/SBA-16 (Pt/CZFe($x$)/SBA) catalysts.

The samples were characterized by X-ray fluorescence analysis (XRF; Supermini200, Rigaku) to confirm the catalysts composition. The Brunauer–Emmett–Teller (BET) specific surface area was measured at −196°C using N_2 (Micromeritics Tristar 3000, Shimadzu). The crystal structure was identified by X-ray powder diffraction (XRD) measurement using Cu-Kα radiation (40 kV, 30 mA) in the 2θ range between 10 and 70 deg. with a step-scanning mode (SmartLab, Rigaku). H_2 temperature programmed reduction (TPR) was conducted under a 5vol%H_2-95vol%Ar gas flow (50 mL·min^{-1}) at the heating rate of 5°C·min^{-1} (BELCAT-B, MicroTracBEL).

Subsequently, the oxygen storage capacity (OSC) was investigated using the reduced sample by the pulse-injection method at 500°C (BELCAT-B, MicrotracBEL). X-ray photoelectron spectroscopy (XPS) analysis was carried out using Al-Kα radiation (PHI5000 Versa Probe II, ULVAC-PHI), and the spectra were fitted using Shirley background and Gaussian-Lorentzian line shape. The acidity was evaluated using a temperature-programmed desorption method using ammonia (NH_3-TPD). After the sample (0.1 g) was preheated at 800°C for 1 h under a helium flow at 50 mL·min^{-1}, it was exposed to ammonia (0.5vol% ammonia–99.5vol% helium, 50 mL·min^{-1}) at 50°C for 30 min, followed by purging at the same temperature for 15 min under a helium flow (50 mL·min^{-1}). Subsequently, the temperature was increased at a rate of 10°C·min^{-1} under a helium flow of 30 mL·min^{-1} (BELCAT-B, MicrotracBEL).

The catalytic oxidation reaction of glycerol in liquid-phase was carried out using an open-air batch reactor, in which an ethanol-cooled condenser (4°C) was equipped to suppress evaporation (Figure 1-1). An aqueous solution of 1wt% glycerol was prepared by dissolving glycerol (Kishida Chemical, 99.0%) in deionized water. The catalyst (0.3 g) and 1wt% glycerol aqueous solution (10

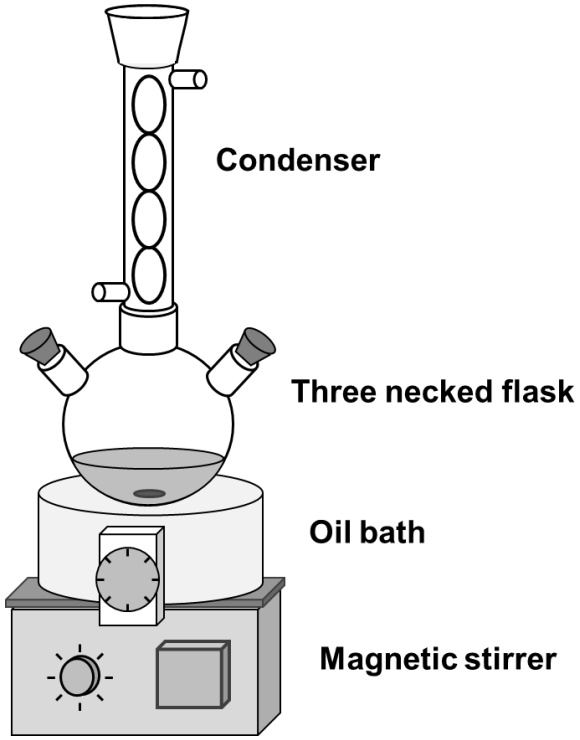

Figure 1-1. Schematic view of the open-system reactor for liquid-phase oxidation.

mL) were mixed in a flask equipped with a condenser (4°C) and stirred in an oil bath at 30°C under the base-free condition (pH = 7) without applying pressure or gas bubbling. After the reaction, the liquid-phase (10 μL) was analyzed using a high-performance liquid chromatography (HPLC, JASCO), where the product was separated by a Shodex Sugar SH-1011 column operating at 50°C with 5 mmol·L^{-1} dilute sulfuric acid as the eluent (prepared by diluting concentrated sulfuric acid (Kishida Chemical, 98%) in deionized water) (0.75 mL·min^{-1}) and detected by a refractive index (RI) and a photodiode array (PDA). The glycerol conversion, product yield, product selectivity, carbon mass balance were estimated as follows:

$$\text{(Glycerol conversion)} = 1 - ([\text{Glycerol}]/[\text{Glycerol}]_0)$$

$$\text{(Product yield)} = ([\text{Product}] \times n_{c,\text{product}})/([\text{Glycerol}]_0 \times n_{c,\text{glycerol}})$$

$$\text{(Product selectivity)} = \text{(Product yield)}/\text{(Glycerol conversion)}$$

$$\text{(Carbon mass balance)} = \Sigma\text{(Product yield)}/\text{(Glycerol conversion)}$$

where $[\text{Glycerol}]_0$ and [Glycerol] are the glycerol concentrations (mol·L^{-1}) before and after the reaction, respectively. [Product] is the product concentration (mol·L^{-1}) and $n_{c,\text{product}}$ and $n_{c,\text{glycerol}}$ values are the number of carbon atoms in the product and glycerol ($n_{c,\text{glycerol}} = 3$), respectively. Each concentration was determined using the calibration curve method, in which standard solutions were prepared by diluting DL-glyceric acid (Tokyo Chemical Industry, 20% in water) with deionized water, by dissolving 1,3-dihydroxyacetone dimer (Sigma-Aldrich, 97%), DL-glyceraldehyde (Sigma-Aldrich, ≥90%), glycolic acid (FUJIFILM Wako Pure Chemical, 97%), oxalic acid dihydrate (Kishida Chemical, 99.5%), and tartronic acid (Alfa Aesar, 98%) in deionized water, and by dissolving sodium β-hydroxypyruvate hydrate (Sigma-Aldrich, ≥97%) and sodium mesoxalate monohydrate (Sigma-Aldrich, ≥ 98%) in dilute sulfuric acid (5 mmol·L^{-1}).

1.3. Results and Discussion

The composition determined by XRF and surface area of the Pt/CZFe(x)/SBA catalysts with the data of SBA are shown in Table 1-1. The measured compositions of Pt/CZFe(x)/SBA were in good agreement with the feed values. The loading of Pt and CZFe(x) obviously lowered the surface area compared to SBA, while similar surface area were obtained for Pt/CZFe(x)/SBA, irrespective of x.

Table 1-1. Measured composition and surface area of the Pt/CZFe(x)/SBA (x = 0, 0.1, 0.2, 0.3) catalysts with the data of SBA

Catalyst	Measured composition	Surface area / $m^2 \cdot g^{-1}$
SBA	-	561(3)
Pt/CZ/SBA	7.2wt%Pt/16.1wt%$Ce_{0.80}Zr_{0.20}O_2$/SBA	286(1)
Pt/CZFe(0.1)/SBA	6.7wt%Pt/17.0wt%$Ce_{0.72}Zr_{0.16}Fe_{0.10}O_{2-\delta}$/SBA	280(1)
Pt/CZFe(0.2)/SBA	6.7wt%Pt/15.3wt%$Ce_{0.64}Zr_{0.15}Fe_{0.21}O_{2-\delta}$/SBA	277(1)
Pt/CZFe(0.3)/SBA	7.0wt%Pt/15.9wt%$Ce_{0.56}Zr_{0.14}Fe_{0.30}O_{2-\delta}$/SBA	274(1)

Figure 1-2 shows the XRD patterns of Pt/CZFe(x)/SBA catalysts. The diffraction peaks of the catalysts were indexed to Pt, the cubic fluorite-type phase, and SBA-16. The peaks of the fluorite-type phase were shifted to higher angles with increasing x up to x = 0.2, suggesting the replacement of the Ce^{4+} (0.111 nm [42]) and Zr^{4+} (0.098 nm [42]) sites for the smaller ionic-size of $Fe^{3+/2+}$ (Fe^{3+}: 0.092 nm, Fe^{2+}: 0.106 nm [42]). For the sample with x = 0.3, no further peak shift was observed compared to that of x = 0.2, where excess Fe component might exist as an amorphous phase because additional crystalline phase was not detected. Therefore, the solid solubility limit is considered to be x = 0.2. As for the Pt phase, the crystallite size was estimated using Scherrer equation. For $x \leq 0.2$,

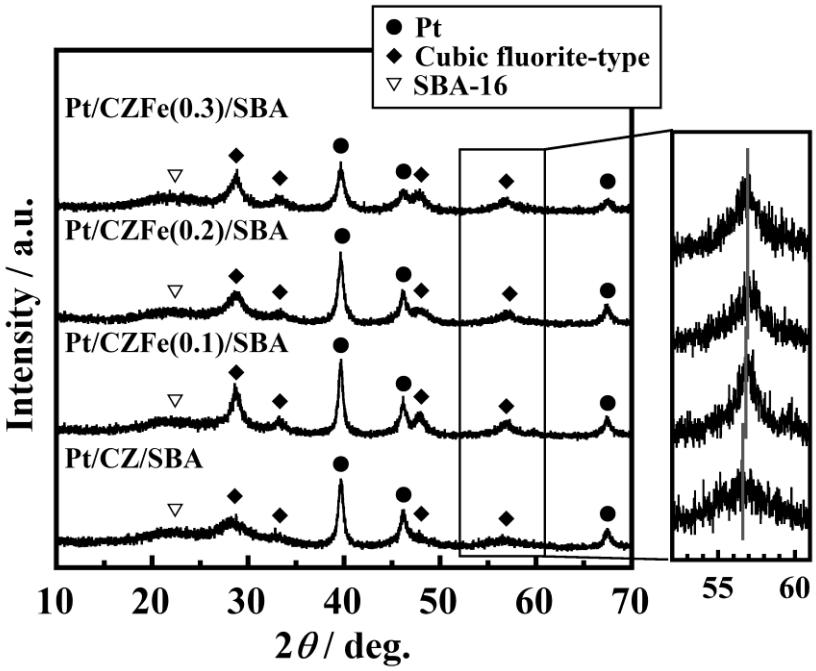

Figure 1-2. XRD patterns of the Pt/CZFe(x)/SBA (x = 0, 0.1, 0.2, 0.3) catalysts.

the Pt crystallite size was slightly decreased with the increasing x: Pt/CZ/SBA (12.1 nm) > Pt/CZFe(0.1)/SBA (11.2 nm) > Pt/CZFe(0.2)/SBA (10.9 nm).

To investigate the oxygen release and storage abilities of the CZFe(x)/SBA ($x \leq 0.2$), TPR and OSC measurements were performed. Here, for the TPR measurements, the promoters are forced to be reacted with hydrogen in 5vol%H_2-95vol%Ar. In other words, the promoters are irreversibly reduced during the TPR measurement. Similarly, the OSC examination irreversibly oxidizes the promoters after the TPR measurement. On the other hand, during the catalytic glycerol oxidation using the Pt loaded on promoters, whenever the active oxygen species is supplied from inside the lattice toward the Pt activator, the formed oxygen vacancies can be compensated by the uptake of the oxygen molecule as oxide ion. That is, the catalyst can be regenerated. Therefore, while the TPR and OSC results are not the direct evidence to explain the glycerol oxidation, the relative comparison of the oxygen release and storage abilities among the prepared promoters can be discussed.

Figure 1-3 shows the TPR profiles of CZFe(x)/SBA ($x \leq 0.2$) with the data of CZ/SBA [43], and the reduction temperatures are provided in Table 1-2. All the samples have the reduction peak and the temperature was lowered with the increase of x. After the TPR analysis, OSC values were obtained from CZFe(x)/SBA ($x \leq 0.2$), and the results are also summarized in Table 1-2. With increasing x, the OSC value was enhanced [43]. From these results, it is demonstrated that the introduction of $Fe^{3+/2+}$ into CZ/SBA successfully improved the oxygen release and storage abilities, due to the formation of the oxide ion vacancies and the synergistic redox between $Ce^{4+/3+}$ and $Fe^{3+/2+}$ [40].

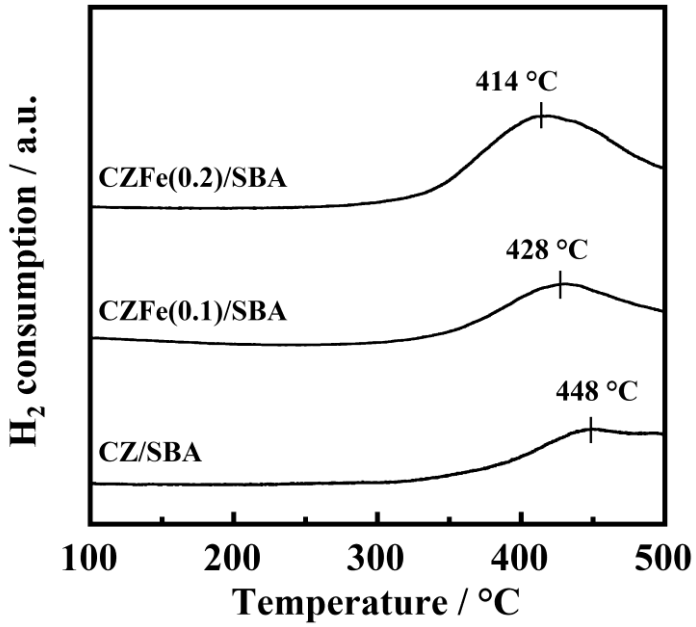

Figure 1-3. TPR profiles of the CZFe(x)/SBA (x = 0, 0.1, 0.2) samples.

Table 1-2. Reduction peak temperature and OSC value of the CZFe(x)/SBA samples

Sample	Reduction temperature / °C	OSC value / μmol $O_2 \cdot g^{-1}$
CZFe(0.2)/SBA	414	94
CZFe(0.1)/SBA	428	42
CZ/SBA	448	17

For Pt/CZFe(0.2)/SBA, and Pt/CZ/SBA, the oxidation state of surface Pt were investigated by XPS. Figure 1-4 presents the XPS results of the Pt 4f core level. For all the catalysts, the binding energies were fitted by the Pt $4f_{7/2}$ and $4f_{5/2}$ of Pt^{2+} and Pt^0, and the $Pt^{2+}/(Pt^0+Pt^{2+})$ ratios were estimated from the peak areas related to Pt^{2+} and Pt^0 in the XPS spectra. The $Pt^{2+}/(Pt^{2+}+Pt^0)$ ratio in Pt/CZFe(0.2)/SBA (52%) was considerably higher than that in Pt/CZ/SBA (35%). These results indicate that the introduction of $Fe^{3+/2+}$ into CZ/SBA contributed to the oxidation of the surface Pt species, where it was reported that the reducibility of CeO_2 generated the oxidized Pt species: $Pt^0 + 2Ce^{4+} \rightarrow Pt^{2+} + 2Ce^{3+}$ [44]. In other words, the efficient oxygen supply from the CZFe(0.2)/SBA is considered to cause the oxidation of the Pt activator. Also, the Pt oxidation can suppress the aggregation, leading to the decrease of the Pt particle size, supported by the results of Pt crystallite size (Figure 1-2).

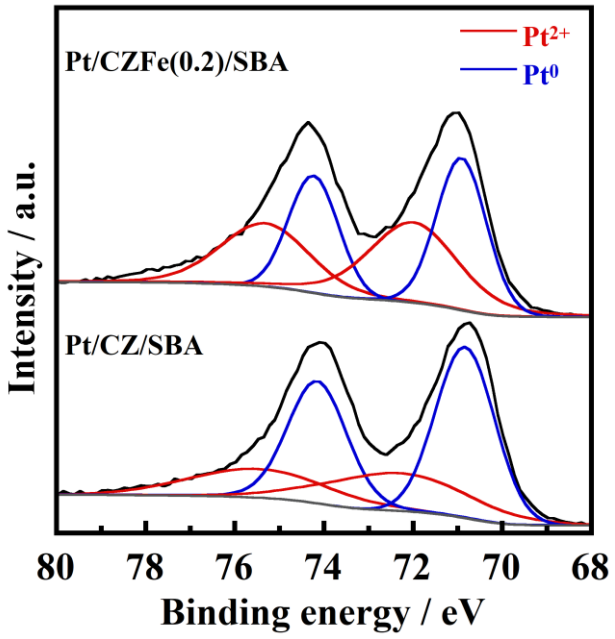

Figure 1-4. XPS spectra of Pt 4f core level for Pt/CZFe(0.2)/SBA and Pt/CZ/SBA.

The GLA yield may be also affected by the acidity, because the acidity is reported to facilitate desorption of GLA, resulting in the suppression of the further oxidation of GLA to GA [2]. Therefore, the acidity was measured by NH_3-TPD, and the profiles of CZFe(x)/SBA ($x \leq 0.2$) are depicted in Figure 1-5. The profiles have three peaks at ca. 150°C, ca. 300°C, and ca. 400°C, which are assigned as the weak, medium, and strong acidic sites on the promoter, respectively. The number of acidic sites were estimated to be CZFe(0.2)/SBA (213 μmol·g^{-1}) > CZFe(0.1)/SBA (158 μmol·g^{-1}) > CZ/SBA (154 μmol·g^{-1}). This improvement of the acidity is related to the oxygen vacancies, formed by the replacement of the Ce^{4+} and Zr^{4+} sites for lower-valent $Fe^{2+/3+}$; that is, the oxygen vacancies were considered to work as Lewis acidic sites.

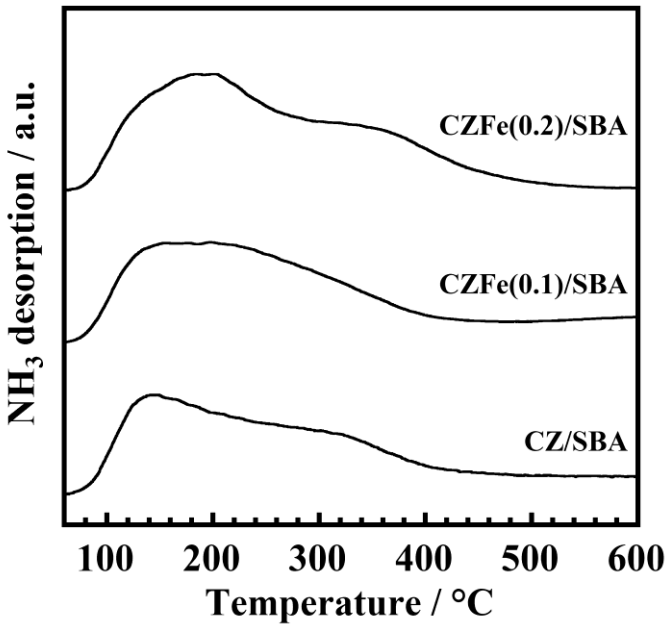

Figure 1-5. NH_3-TPD profiles of the CZFe(x)/SBA (x = 0, 0.1, 0.2) samples.

For the Pt/CZFe(x)/SBA catalysts, the catalytic liquid-phase oxidation of glycerol was performed at 30°C under the atmospheric air pressure for 4 h, and the glycerol conversion and the GLA yield are depicted in Figure 1-6. In the range of $x \leq 0.2$, the glycerol conversion increased with increasing x, because the oxygen supply from the promoter facilitated the oxidation of glycerol. By the increase of the glycerol conversion, the GLA yield was simultaneously increased up to $x = 0.2$. This enhancement of the GLA yield might be also caused by the increase of the acidity of the promoter. On the other hand, excess introduction of $Fe^{3+/2+}$ ($x = 0.3$) decreased the glycerol conversion involved with the decrease of the GLA yield, because the number of active sites might be decreased by the amorphous impurity phase. Therefore, the optimum composition for the GLA production is determined to be Pt/CZFe(0.2)/SBA, and the GLA yield reached up to 22.1%.

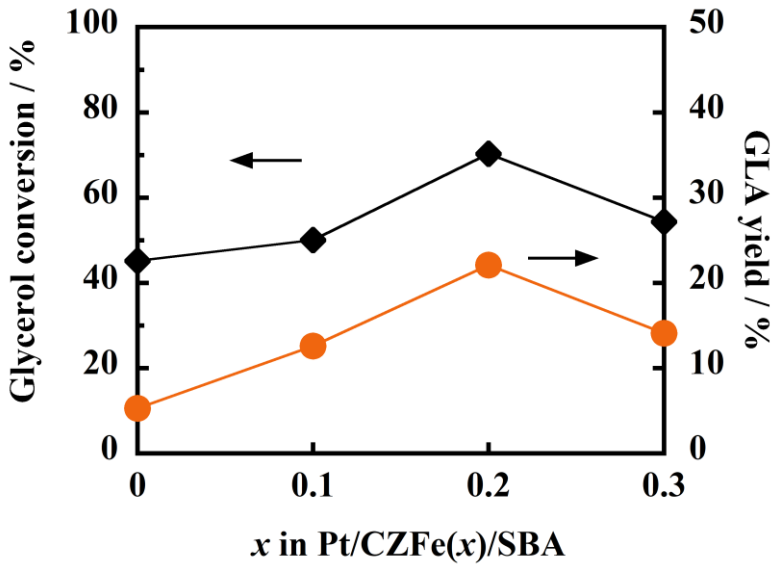

Figure 1-6. Glycerol conversion and GLA yield as a function of Fe content (x) for Pt/CZFe(x)/SBA at 30°C under the atmospheric air.

For Pt/CZFe(0.2)/SBA, in order to discuss the reaction routes, the glycerol conversion and the product yields as a reaction time function was examined. As possible candidates, the yields of GA, DHA, GLOA, HA, TA (tartronic acid), MA (mesoxalic acid), OA were evaluated. The results are presented in Figure 1-7. The glycerol conversion was continuously increased with increasing the reaction time. After the reaction for 1 h, the order of the yield was GLA (10.8%) > GA (5.0%) > DHA (3.9%) > GLOA (1.8%), where HA, TA, MA, and OA were not detected. Thus, the primary oxidation of glycerol predominantly proceeded to generate GLA rather than the secondary oxidation to DHA. Also, further oxidation to GA and GLOA occurred simultaneously. Subsequently, the GLA yield was gradually increased up to 4 h, and then decreased due to the conversion of GLA to GA. For the chemically stable compound of GA, the yield was monotonically increased, which caused the slight increase of the further oxidation product yields of GLOA, HA, TA, and OA, while MA was not detected. As for the DHA production, since the yield constantly showed the low values (ca.

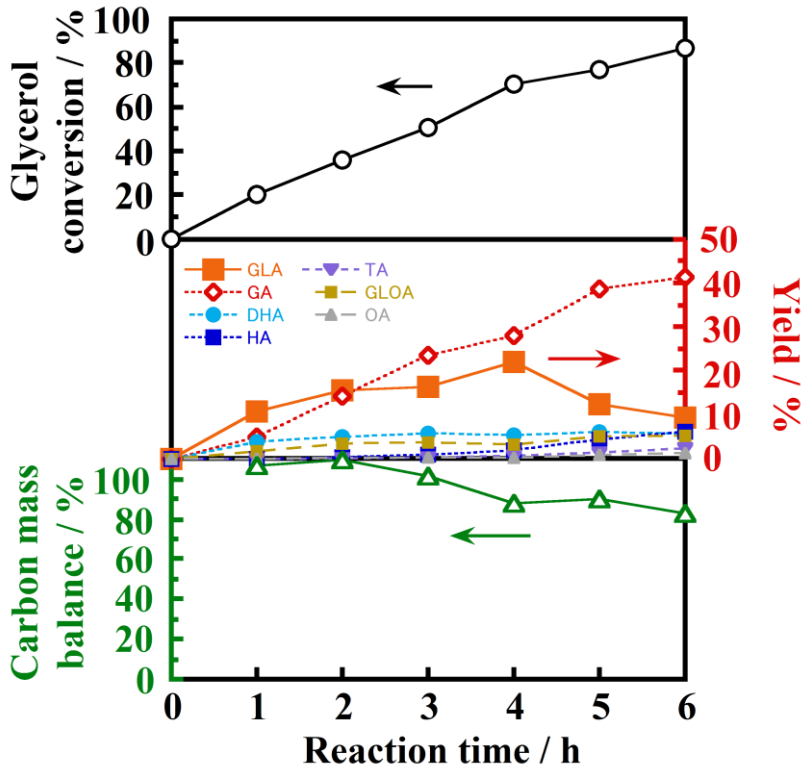

Figure 1-7. Dependence of glycerol conversion, product yields, and carbon mass balance on reaction time in the selective oxidation of glycerol using Pt/CZFe(0.2)/SBA at 30°C under the atmospheric air.

6%), further oxidation of DHA also proceeded continuously. Carbon mass balance maintained ca. 100% up to 3 h, while it decreased after 3 h. This decrease of the mass balance is related to the generation of carbon dioxide and/or the adsorption of some products.

From these results, the highest GLA yield (22.1%) with high glycerol conversion (70.3%) was demonstrated by the reaction time for 4 h. The GLA yield of Pt/CZFe(0.20)/SBA (22.1%) is comparable with that of the previous Pt/CNTs catalyst (22.8%) [15] which requires the control of the reaction temperature (60°C) and the pure oxygen gas bubbling (150 $mL \cdot min^{-1}$). Therefore, it is clear that Pt/CZFe(0.2)/SBA can effectively convert glycerol to GLA even at around room temperature under the atmospheric air pressure without flowing oxygen gas.

1.4. Conclusion

In this chapter, for the production of glyceraldehyde from glycerol effectively at around room temperature under the atmospheric air pressure, Pt/CeO_2–ZrO_2–Fe_2O_3/SBA-16 catalysts were applied. The introduction of Fe_2O_3 into the CeO_2–ZrO_2 lattice improved the oxygen release and storage abilities, which facilitated the oxidation of glycerol even under the moderate condition. the highest activity was obtained for 7wt%Pt/16wt%$Ce_{0.64}Zr_{0.16}Fe_{0.20}O_{2-\delta}$/SBA-16, which exhibited the high glyceraldehyde yield (22.1%) with high glycerol conversion (70.3%) after the reaction for 4 h under the considerably moderate condition of 30°C under the atmospheric air pressure, while the previously reported Pt/carbon nanotubes catalyst required more severe reaction condition (60°C, 150 $mL \cdot min^{-1}$ of pure oxygen gas bubbling) to obtain GLA yield of 22.8%.

Chapter 2

Effective production of glyceric acid from glycerol

2.1. Introduction

In Chapter 1, the 7wt%Pt/16wt%$Ce_{0.64}Zr_{0.16}Fe_{0.20}O_{2-\delta}$/SBA-16 catalyst could effectively convert glycerol into GLA after the reaction for 4 h at 30°C under atmospheric air pressure, and the GLA yield was 22.1%. Here, some value-added chemicals can be also detected (Figure 1-6), and GA was generated with high yield of 28.0%.

GA has drawn attention in the medical field [45], because GA and its derivatives have been reported to show biological activities; e.g., the antitrypsin activity [46], acceleration of acetaldehyde and ethanol metabolism [47], improvement of the viability of ethanol-exposed cells [48], and activation of proliferation of dermal cells [49]. GA is also used in the production of amino acids, such as serine [5].

Previously, there are many reports to produce GA by using fermentation method [50-53]. According to Habe et al., by using *Gluconobacter frateuri* and *Acetobacter trapicalis*, D-GA was obtained with 72% ee (enantiomeric excess) and 99% ee, respectively. Gerstenbruch et al. reported that D-GA was produced from glycerol via GLA in a two-step enzyme reaction with the FAD-dependent alditol oxidase from *Streptomyces coelicolor* [54], where the oxidation of 30 mM glycerol resulted in 15.7 mM GA and 3 mM GLA after 40 h at 37℃ with adding catalase in 100 mM bicine buffer pH 9.0.

As for the catalytic oxidation, since GA is chemically stable, many studies have been reported; however, most of them require the addition of base (NaOH, etc.) and/or high pressure of

pure O_2 gas. Although the conditions of base-free and air conditions under the atmospheric pressure are favorable from the economical point of view, only few studies were reported; e.g., Pt/C showed the high GA yield of 55% (glycerol conversion: 90%) in pH = 7 under the atmospheric pressure (air flow at 0.75 $mL \cdot min^{-1}$) at 60°C [17].

Therefore, Chapter 2 aims to obtain GA with high efficiency, based on the results in Chapter 1. The high GLA yield is attributed to the phenomenon that the effective oxygen supply from CeO_2–ZrO_2–Fe_2O_3 toward Pt facilitated the glycerol oxidation, whereas moderate condition could suppress the further oxidation of GLA. In addition, the GLA yield might be also affected by the acidic sites on the CeO_2–ZrO_2–Fe_2O_3 promoter, because the acidity of catalyst supports is reported to accelerate desorption of GLA, resulting in the suppression of the further oxidation of GLA to GA [2]. These considerations suggest that the important factors to show the high GA yield are the increase in the oxygen release and storage abilities, even under moderate conditions, and the lowering of the amount of acidic sites. A simple and effective method to achieve these factors is to increase the loading amount of CeO_2–ZrO_2–Fe_2O_3 compared to the case in Chapter 1. The increase in the amount of CeO_2–ZrO_2–Fe_2O_3 promoter is considered to enhance the oxygen release and storage abilities of CeO_2–ZrO_2–Fe_2O_3/SBA-16. Furthermore, the acidic sites on the promoter surface are expected to be lowered by particle growth due to the high loading amount of CeO_2–ZrO_2–Fe_2O_3.

In this chapter, the CeO_2–ZrO_2–Fe_2O_3 loading amount in Pt/CeO_2–ZrO_2–Fe_2O_3/SBA-16 was increased to produce GA effectively, and their catalytic activities for selective glycerol oxidation were investigated under moderate conditions of the atmospheric open-air system at room temperature of 30°C.

2.2. Experimental Procedure

$Ce_{0.64}Zr_{0.16}Fe_{0.20}O_{2-\delta}$/SBA-16 was synthesized using a co-precipitation technique with the same method described in Chapter 1, where the $Ce_{0.64}Zr_{0.16}Fe_{0.20}O_{2-\delta}$ loading amount (*x*) varied from 0 to 60wt%, and the samples were denoted as *x*wt%CZFe/SBA. Pt loading onto *x*wt%CZFe/SBA was carried out using the impregnation procedure according to Chapter 1 to obtain 7wt%Pt/*x*wt%$Ce_{0.64}Zr_{0.16}Fe_{0.20}O_{2-\delta}$/SBA-16 (Pt/*x*wt%CZFe/SBA).

The crystalline phase was identified with an XRD (SmartLab, Rigaku) using a Cu-Kα radiation (40 kV, 30 mA). The XRD data were analyzed by whole powder pattern fitting using PDXL software (Rigaku) to estimate the crystallite size. The lattice constant was calculated by refining the XRD peak angles using α-alumina as an internal standard. The BET specific surface area was measured at −196°C using N_2 (Micromeritics Tristar 3000, Shimadzu). TPR and OSC measurements were conducted as described in Chapter 1. The TPR profiles were fitted by using Gaussian-Lorentzian line shapes. The acidity was assessed by using NH_3-TPD measurement, according to Chapter 1. The sample composition was determined using XRF (Supermini200, Rigaku). The morphology was observed by transmission electron microscopy (TEM; H-800, Hitachi). XPS was measured using Al-Kα radiation (PHI5000 Versa Probe II, ULVAC-PHI). The catalytic glycerol oxidation test and HPLC analysis were conducted at 30°C in the atmospheric air according to Chapter 1.

2.3. Results and Discussion

Figure 2-1 shows the XRD patterns of *x*wt%CZFe/SBA and SBA [41]. The peaks corresponding to SBA-16 and the cubic fluorite-type structure of $Ce_{0.64}Zr_{0.16}Fe_{0.20}O_{2-\delta}$ (CZFe) were observed for *x*wt%CZFe/SBA, where no impurity phases were detected. The crystallite size of CZFe was estimated, and the relationship between the crystallite size and the CZFe loading amount (*x*) is shown in Figure 2-2. The crystallite size increased with the increase of *x*, suggesting the particle growth. Figure 2-2 also displays the specific surface area, measured by the BET method. The decrease of the surface area was clearly observed with increasing *x*.

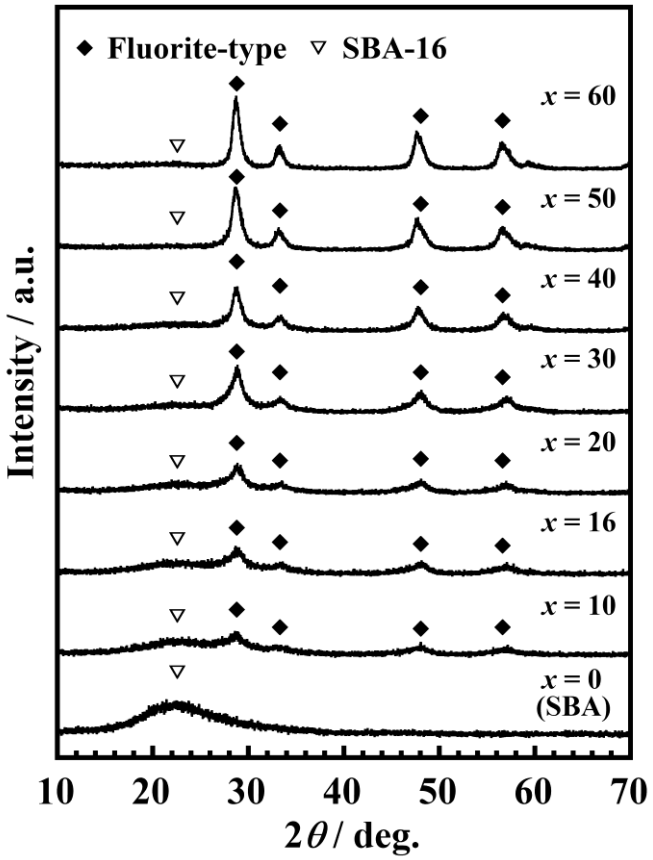

Figure 2-1. XRD patterns of *x*wt%CZFe/SBA.

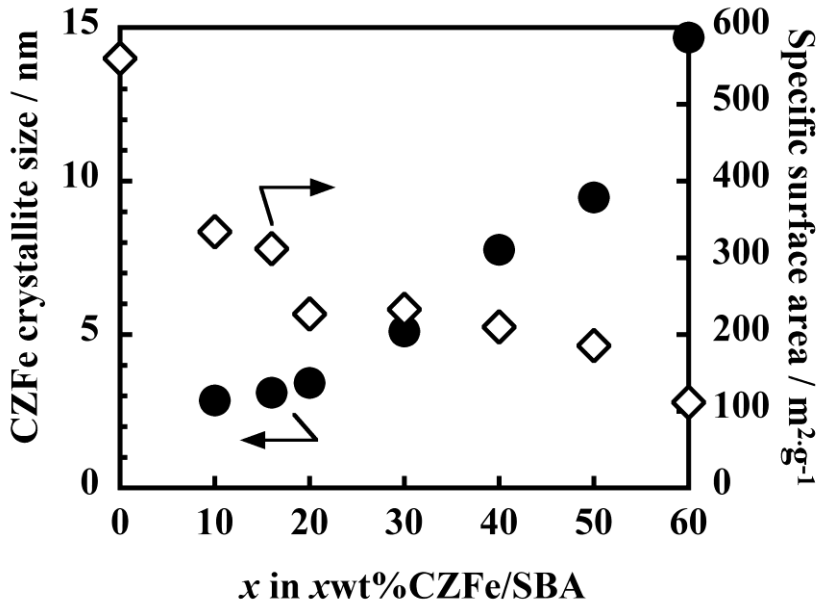

Figure 2-2. Effect of the CZFe loading amount (*x*) on CZFe crystallite size and specific surface area for *x*wt%CZFe/SBA.

To compare the oxygen release and storage abilities of *x*wt%CZFe/SBA, TPR measurements and OSC examination were conducted. The profiles are depicted in Figure 2-3 together with the SBA data. Although SBA demonstrated no reduction peak, the profiles of *x*wt%CZFe/SBA could be fitted to three reduction peaks. Hereafter, the peaks at ca. 400, ca. 440, and ca. 500°C are denoted as the α-peak, β-peak, and γ-peak, respectively. The α- and β-peaks might be respectively attributed to the release of the surface and bulk oxygen species involved with the synergistic reduction of Ce^{4+} to Ce^{3+} with Fe^{3+} to Fe^{2+} [55,56]. The γ-peak is probably assigned to the reduction of Fe^{2+} to Fe^{0} [57], while only its shoulder was observed. The peak top temperatures of the α- and β-peaks, related to the valence change of $Ce^{3+/4+}$ and $Fe^{2+/3+}$, and the peak area ratio of α-peak/(α-peak+β-peak) are summarized in Table 2-1. While the reduction temperatures of the α- and β-peaks were almost unchanged, the α-peak/(α-peak+β-peak) ratio decreased with increasing the CZFe loading amount (*x*). In other words, the increase of *x* decreases the effects of the surface oxygen release and increases the effects of the bulk oxygen release. This behavior is caused by the particle growth of the CZFe

promoter. Table 2-1 tabulates the total hydrogen consumption amount. The total amount of hydrogen consumption increased monotonically with increasing *x*. Figure 2-4 shows the OSC values for *x*wt%CZFe/SBA. Each OSC value was consistent with that of the total amount of oxygen released in the TPR measurements. The OSC value was linearly improved with the increase of *x*, similar to the tendency exhibited by the total hydrogen consumption amount (Table 2-1). Therefore, the oxygen release and storage abilities were continuously enhanced with the increase of *x*. For further investigation, the OSC per gram of CZFe was estimated, and the results are also depicted in Figure 2-4. OSC per CZFe was almost unchanged, suggesting that the oxygen species could be stored inside the lattice rather than the surface [40]. Thus, the continuous increase in OSC was predominantly affected by the CZFe loading amount compared to the CZFe surface.

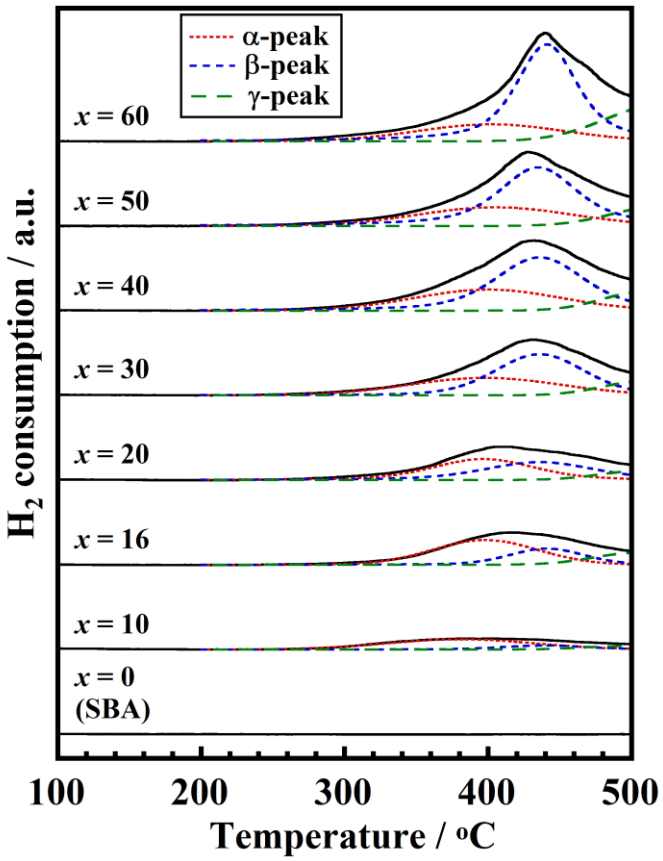

Figure 2-3. TPR profiles of *x*wt%CZFe/SBA.

Table 2-1. Reduction temperatures of α- and β-peaks, peak area ratio of (α-peak)/(α-peak + β-peak), and total amount of H_2 consumption for *x*wt%CZFe/SBA

Sample	Reduction temperature / °C		α-peak /(α-peak+β-peak) ratio / %	Total amount of H_2 consumption / μmol·g^{-1}
	α-peak	β-peak		
x = 0	-	-	-	0
x = 10	381	440	80	119
x = 16	398	441	66	224
x = 20	397	436	51	260
x = 30	398	436	39	370
x = 40	400	436	35	450
x = 50	405	435	32	481
x = 60	402	441	25	628

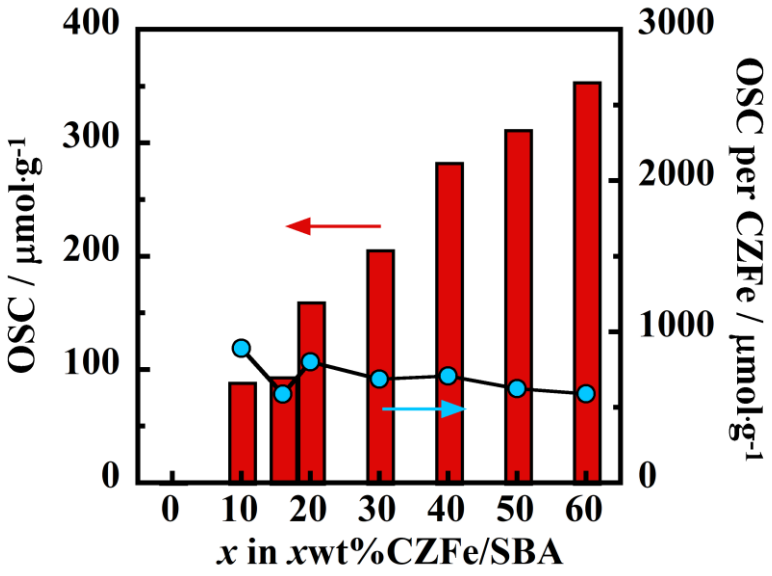

Figure 2-4. Effect of the CZFe loading amount (*x*) on OSC and OSC per CZFe for *x*wt%CZFe/SBA.

For CZFe/SBA, as low acidity is necessary to produce GA effectively, NH_3-TPD measurements were carried out. Figure 2-5 shows the NH_3-TPD profiles of the *x*wt%CZFe/SBA samples. The profile of SBA showed two small peaks at ca. 150°C and ca. 300°C, assigned to the weak and strong acidic sites on the SBA-16 support, respectively. For the CZFe loaded samples, three peaks were observed at ca. 150°C, ca. 300°C, and ca. 400°C, corresponding to the weak, medium, and strong acidic sites on the CZFe promoter, respectively. From these profiles, the total number of acidic sites was calculated, and the results are shown in Figure 2-6. The number of acidic sites increased up to x = 16, indicating that the CZFe promoter exhibits a high acidity. The CZFe system was reported to have oxygen vacancies formed by the replacement of the Ce^{4+} and Zr^{4+} sites for lower-valent $Fe^{2+/3+}$ [40], which might work as Lewis acidic sites. For x > 16, the number of acidic sites decreased with increasing x. To exclude the effect of the CZFe loading amount, the number of acidic sites per gram of CZFe was estimated (Figure 2-6). As x increased, the number of acidic sites per CZFe significantly decreased, as these acidic sites were intrinsically related to the surface area and impacted by the particle growth. Thus, the lowering of the acidity for x > 16 was

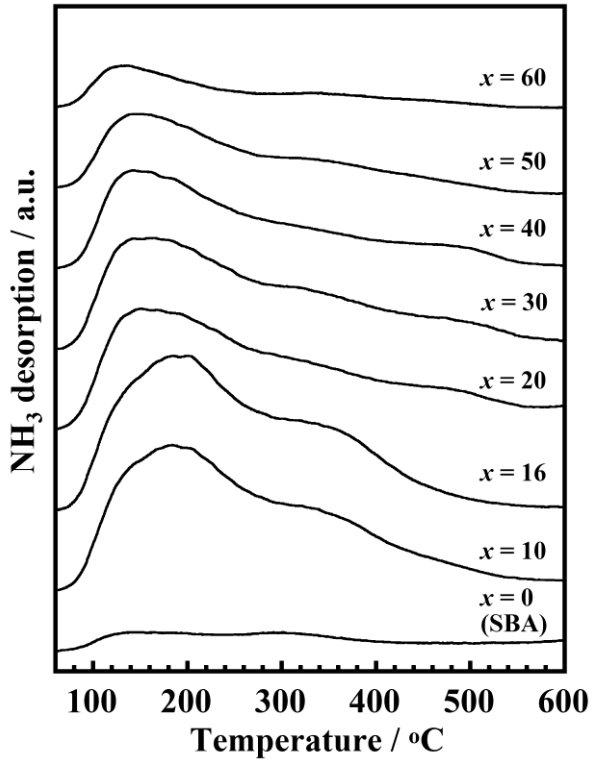

Figure 2-5. NH_3-TPD profiles of *x*wt%CZFe/SBA.

predominantly affected by the CZFe surface compared to the CZFe loading amount. Therefore, the increase in the CZFe loading amount successfully lowered the acidity of CZFe in the range of x > 16. Therefore, the high loading amount of CZFe contributed to the lowering of the acidic sites as well as the improvement of the oxygen release and storage abilities as expected.

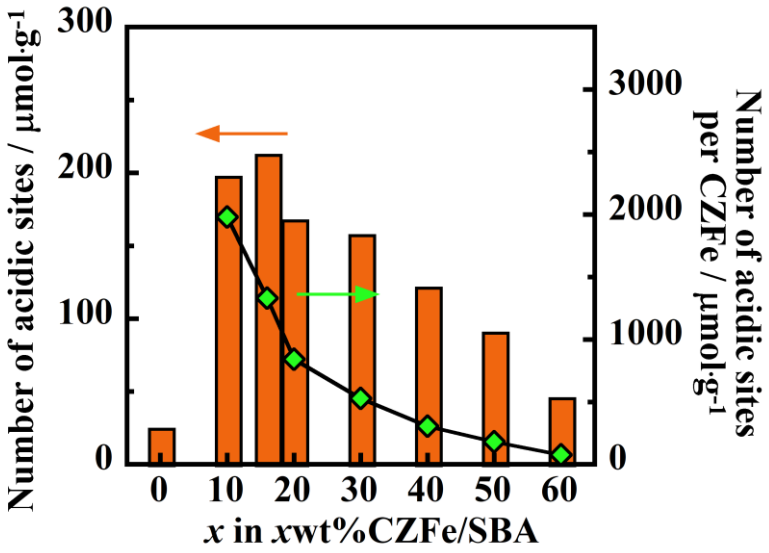

Figure 2-6. Effect of the CZFe loading amount (x) on number of acidic sites and number of acidic sites per CZFe for $x$wt%CZFe/SBA.

Figure 2-7 shows the XRD patterns of Pt-loaded $x$wt%CZFe/SBA. All the peaks were indexed as metallic Pt, the fluorite-type structure of CZFe, and SBA-16. The crystallite sizes of Pt and CZFe were estimated from the XRD patterns, and the results are shown in Figure 2-8. The CZFe crystallite sizes in Pt/$x$wt%CZFe/SBA were almost the same as those in the case of $x$wt%CZFe/SBA (Figure 2-2); that is, the Pt loading process did not change the CZFe crystallite size. As for the Pt crystallite size, the value decreased with increasing x. This phenomenon indicates that the oxygen supply from the CZFe promoter facilitated the oxidation of Pt, which contributed to the suppression of the Pt particle growth, similar to that reported by a previous study [58].

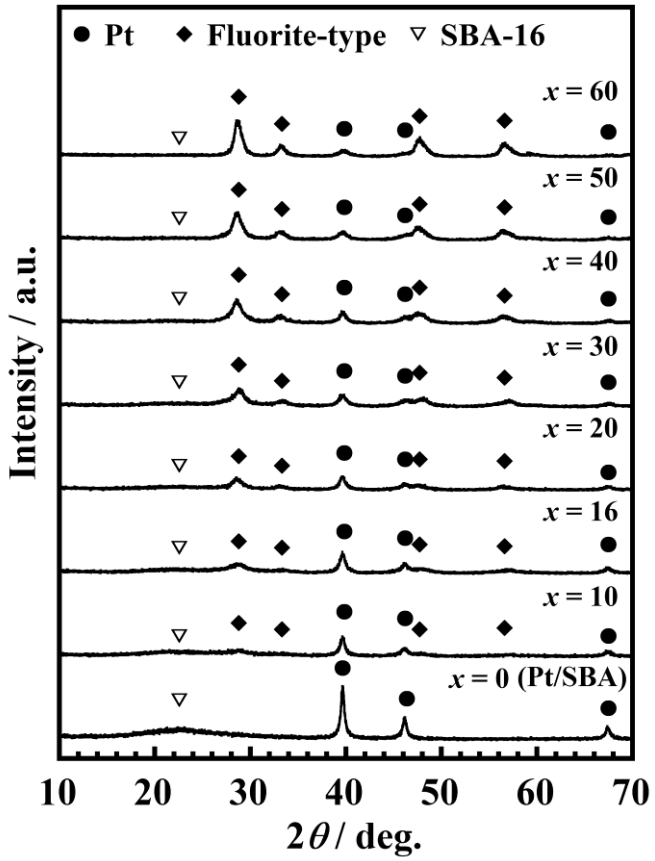

Figure 2-7. XRD patterns of Pt/*x*wt%CZFe/SBA.

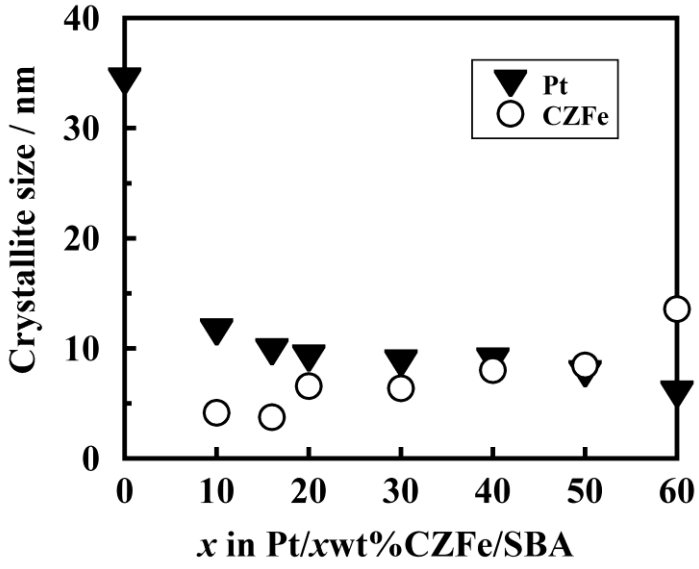

Figure 2-8. Crystallite sizes of CZFe and Pt as a function of the CZFe loading amount (*x*) for Pt/*x*wt%CZFe/SBA.

The compositions of Pt/*x*wt%CZFe/SBA measured by XRF analysis were in good agreement with their feed values within the range of experimental error (Table 2-2). The specific surface area, estimated by the BET method (Table 2-2), decreased with increasing *x*. Furthermore, the Pt loading of Pt/*x*wt%CZFe/SBA caused a decrease in the specific surface area compared to that of the *x*wt%CZFe/SBA (Figure 2-2).

Table 2-2. Measured composition and specific surface area of Pt/*x*wt%CZFe/SBA

Catalyst	Measured composition	Specific surface area / $m^2 \cdot g^{-1}$
Pt/SBA	7.1wt%Pt/SBA-16	476(1)
Pt/10wt%CZFe/SBA	7.9wt%Pt/9.9wt%$Ce_{0.58}Zr_{0.17}Fe_{0.24}O_{2-\delta}$/SBA-16	286(1)
Pt/16wt%CZFe/SBA	6.7wt%Pt/15.3wt%$Ce_{0.64}Zr_{0.15}Fe_{0.21}O_{2-\delta}$/SBA-16	277 (1)
Pt/20wt%CZFe/SBA	7.0wt%Pt/19.6wt%$Ce_{0.67}Zr_{0.15}Fe_{0.17}O_{2-\delta}$/SBA-16	200(1)
Pt/30wt%CZFe/SBA	7.2wt%Pt/30.8wt%$Ce_{0.63}Zr_{0.17}Fe_{0.20}O_{2-\delta}$/SBA-16	182(1)
Pt/40wt%CZFe/SBA	6.9wt%Pt/41.1wt%$Ce_{0.64}Zr_{0.16}Fe_{0.20}O_{2-\delta}$/SBA-16	169(1)
Pt/50wt%CZFe/SBA	6.8wt%Pt/50.6wt%$Ce_{0.65}Zr_{0.15}Fe_{0.20}O_{2-\delta}$/SBA-16	157(1)
Pt/60wt%CZFe/SBA	6.9wt%Pt/60.3wt%$Ce_{0.64}Zr_{0.15}Fe_{0.21}O_{2-\delta}$/SBA-16	76(1)

TEM photographs and electron diffraction patterns of Pt/*x*wt%CZFe/SBA (*x* = 0, 16, 40, 60) are displayed in Figure 2-9. For Pt/SBA, the regular arrengement of mesopores with ca. 13 nm diameter were confirmed. In addition, the Pt particles with diameters from 10 to 40 nm were observed as dark spots in and/or on the mesopores. On the other hand, Pt/*x*wt%CZFe/SBA (*x* = 16, 40, 60) contains small Pt particles with ca. 10 nm diameter, compared to the Pt/SBA case, similar to the Pt crystallite size (Figure 2-8). While it is difficult to distinguish between CZFe and SBA, the electron diffraction patterns can be assigned to the Pt metal and the fluorite-type structure derived

from CZFe. For the x = 60 catalyst, aggregates were clearly observed outside the mesopores, possiblity becase of the particle aggregation of CZFe.

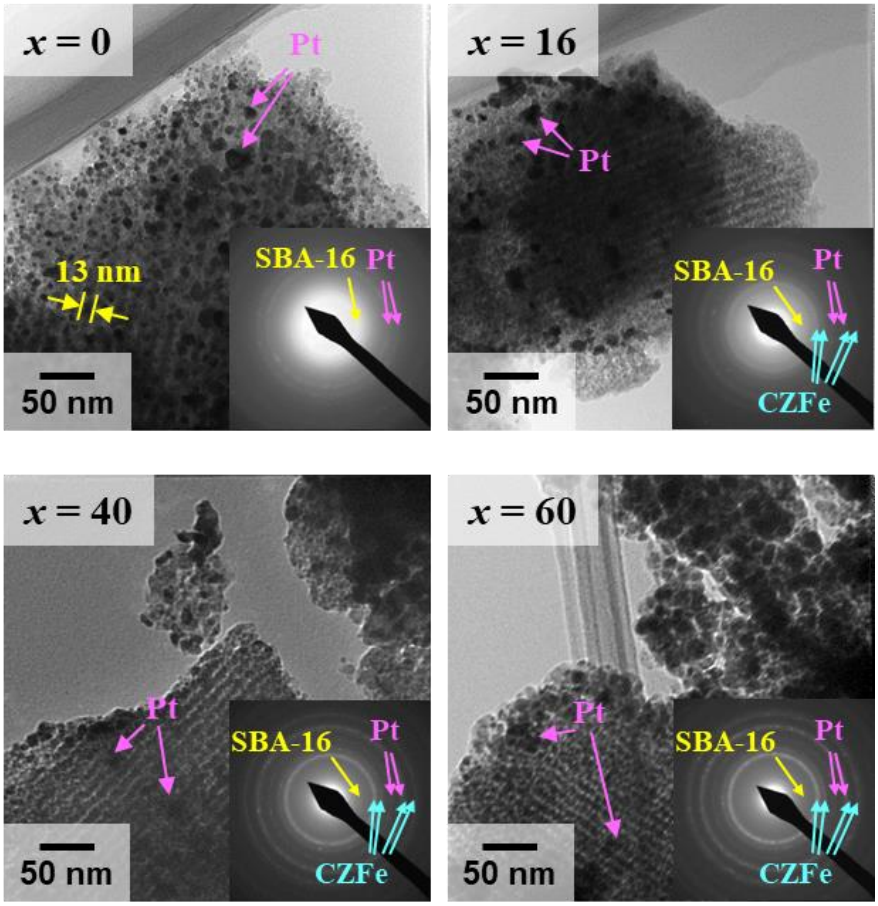

Figure 2-9. TEM images for Pt/$x$wt%CZFe/SBA (x = 0, 16, 40, and 60). Electron diffraction images are shown in the inset.

The XPS spectra of the Pt 4f core levels of Pt/*x*wt%CZFe/SBA (*x* = 0, 16, 40, 60) are shown in Figure 2-10. The peaks were identified as Pt^{2+} and Pt^{0}, and the $Pt^{2+}/(Pt^{2+}+Pt^{0})$ ratio is presented in the figure. The $Pt^{2+}/(Pt^{2+}+Pt^{0})$ ratios of Pt/16wt%CZFe/SBA (52%) was significantly higher than that of Pt/SBA (26%). This phenomenon indicates that the oxygen supply from CZFe contributed to the generation of Pt^{2+}. The *x* = 40 catalyst exhibited the slightly high $Pt^{2+}/(Pt^{2+}+Pt^{0})$ ratio compared to the *x* = 16 case, likely due to the further improvement of the oxygen release and storage abilities. On the other hand, the $Pt^{2+}/(Pt^{2+}+Pt^{0})$ ratio of *x* = 60 was decreased compared to that of *x* = 40 regardless of the further increase of oxygen release and storage abilities. This behavior can be explained by the decrease of the CZFe surface for the Pt loading.

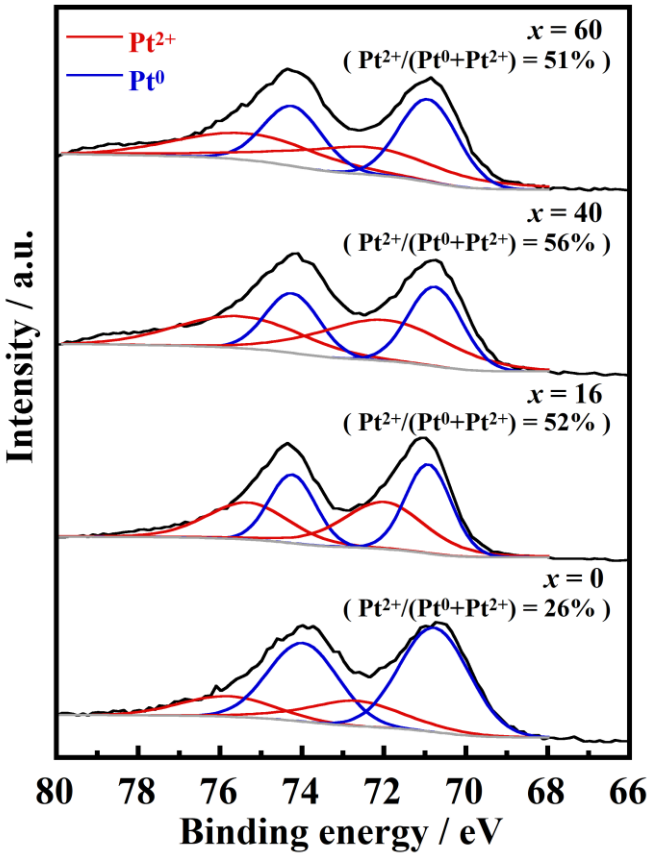

Figure 2-10. XPS spectra of Pt 4f core levels of Pt/*x*wt%CZFe/SBA (*x* = 0, 16, 40, 60).

The catalytic liquid-phase oxidation of glycerol was carried out for Pt/*x*wt%CZFe/SBA at 30°C under the atmospheric air pressure for 4 h. Figure 2-11 shows the glycerol conversion and product yields as a function of the CZFe loading amount. The glycerol conversion increased with increasing *x* up to the catalyst with *x* = 40, while the specific surface area decreased. This behavior indicates that the increase in OSC mainly affected the improvement of the catalytic activity. On the other hand, for *x* > 40, glycerol conversion decreased because the low specific surface area decreased the catalytic active sites. Therefore, the highest glycerol conversion was obtained for the *x* = 40 catalyst. For all the prepared catalysts, the predominant product was GA, which was generated by the oxidation of the primary OH group in glycerol via the intermediate compound of GLA. In addition, the GA yield was higher than that of DHA, which was formed by the oxidation of the secondary OH group in glycerol. This indicates that the primary OH group in glycerol is predominantly oxidized compared to the secondary OH group. For GLA production, the yield

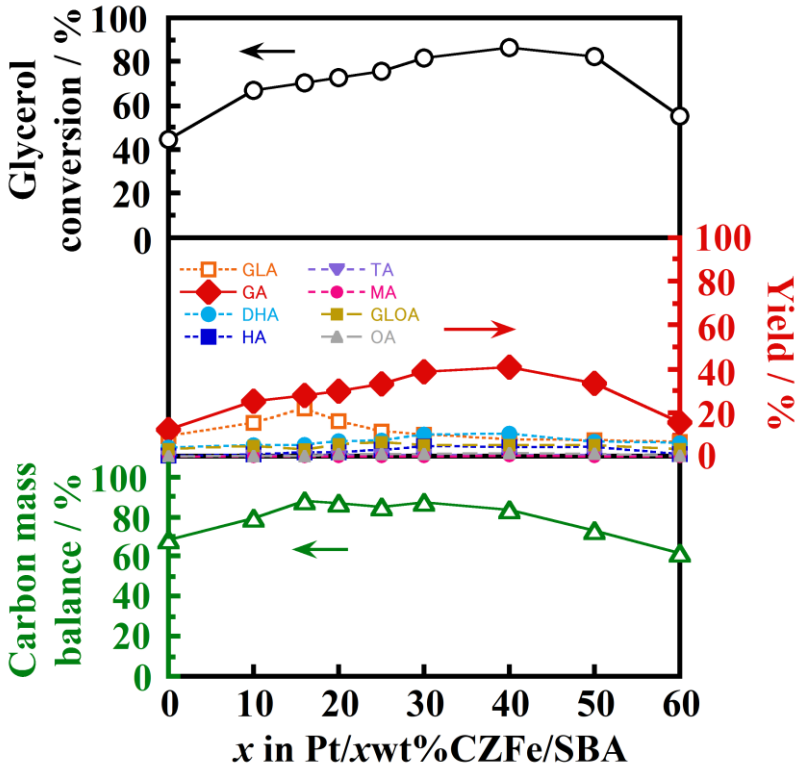

Figure 2-11. Glycerol conversion, product yields, and carbon mass balance as a function of the CZFe loading amount (*x*) for Pt/*x*wt%CZFe/SBA at 30°C in the atmospheric air.

increased with increasing x up to x = 16, whereas the GLA yield decreased in the range of x > 16. This behavior is related to the number of acidic sites and indicated that the lowered acidity of CZFe (x >16) suppressed the GLA desorption, resulting in the acceleration of the further oxidation of GLA to GA. For GA production, the yield continuously increased until x = 40, and the x = 40 catalyst showed the highest GA yield of 40.9%. This high GA yield might be caused by the lowering of the acidity and the increase in the oxygen release and storage abilities. In contrast, the GA yield for x > 40 decreased because of the decrease in glycerol conversion. The yields of the other organic products (HA, TA, MA, GLOA, and OA) were lower than 10%. Carbon mass balance were less than 100% for all the catalysts, implying the further oxidation to carbon dioxide and/or the adsorption of glycerol and some products.

Figure 2-12 shows the catalytic activity for the x = 40 catalyst (Pt/40wt%CZFe/SBA) as a reaction time function at 30°C under the atmospheric air pressure. The glycerol conversion continuously increased with increasing reaction time and reached up to 99.2% after 10 h. The GA yield was higher than that of GLA even after 1 h of reaction, indicating that the further oxidation of GLA was accelerated due to the high oxygen release and storage abilities and the suppression of the desorption of GLA due to the low acidity. Although the DHA yield was constant (ca. 9%) and lower than that of GA, the further oxidized products of GA or DHA (HA, TA, MA, GLOA, and OA) gradually increased. The predominant product was GA, and its yield increased to 68.2% after 10 h of reaction, where the GA selectivity was estimated to be 68.8%. Carbon mass balance after 1 h was ca. 70% likely due to the adsorption of glycerol, while it increased with the time and reached up to ca. 100% after 5 h. Although the previous Pt/C catalyst [17] could generate GA with relatively high yield (55%) at pH = 7 under the atmospheric pressure conditions and flowing air (0.75 $mL \cdot min^{-1}$) at 60°C, the GA yield was higher with the present Pt/40wt%CZFe/SBA catalyst that exhibited superior activity under the moderate conditions of 30°C in the atmospheric open-air system without additives, such as base and gas flow.

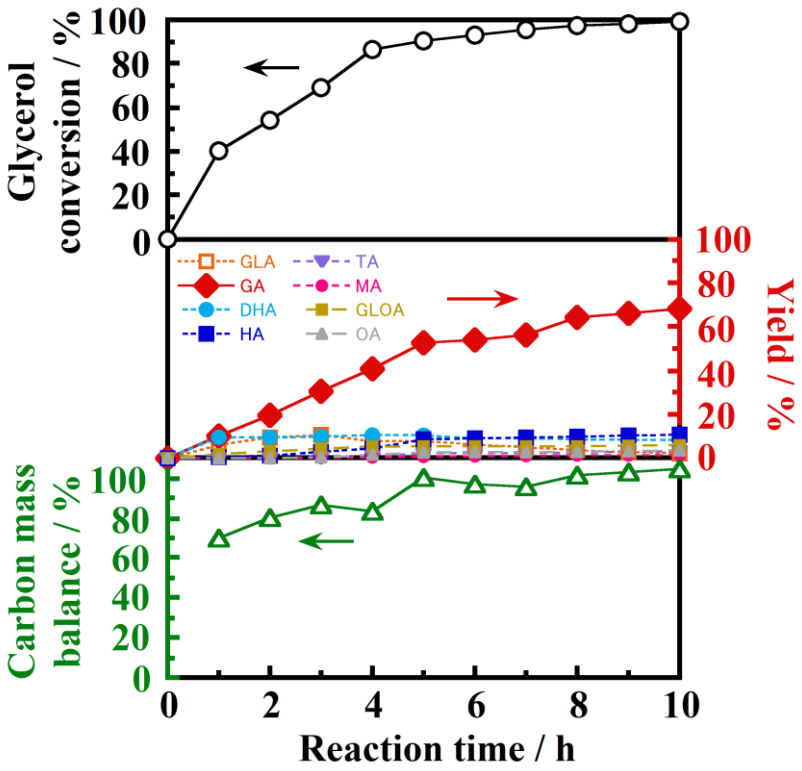

Figure 2-12. Dependence of glycerol conversion, product yields, and carbon mass balance on reaction time in the selective oxidation of glycerol using the *x* = 40 catalyst (Pt/40wt%CZFe/SBA) at 30°C in the atmospheric air.

2.4. Conclusion

In this chapter, it was demonstrated the effective production of GA from glycerol using Pt/CeO_2–ZrO_2–Fe_2O_3/SBA-16 under moderate conditions in an atmospheric open-air system at room temperature without additives, such as base or oxygen gas flow. In the catalysts, the CeO_2–ZrO_2–Fe_2O_3 promoter supported on SBA-16 facilitated the oxidation of the Pt activator. The increase in the CeO_2–ZrO_2–Fe_2O_3 loading amount led to particle growth. As a result, the number of acidic sites of CeO_2–ZrO_2–Fe_2O_3/SBA-16 decreased with increasing loading amount in the range over 16wt%. Conversely, the oxygen release and storage abilities increased continuously even at a high

loading amount of CeO_2–ZrO_2–Fe_2O_3. The low acidity and high oxygen release and storage abilities successfully improved the GA yield, and the highest activity was obtained for 7wt%Pt/40wt%$Ce_{0.64}Zr_{0.16}Fe_{0.20}O_{2-\delta}$/SBA-16, which exhibited a high GA yield (68.2%) and selectivity (68.8%) with glycerol conversion (99.2%) even under moderate conditions after 10 h of reaction in an open-air system at 30°C.

Chapter 3

Novel catalysts for hydroxypyruvic acid production from glycerol

3.1. Introduction

In the previous chapters, the high yields of GLA and GA were demonstrated. This chapter deals with the HA production from glycerol, because HA is an important intermediate in the pharmaceutical industries due to is high functionality; that is, three different functional groups of hydroxyl, carbonyl, and carboxyl groups [5, 59]. In addition, during the synthesis of biologically important molecules using the transketolase enzyme, HA is the widely used donor substrate [60]. For the production of HA, Lenfant et al. reported that HA was generated from D-serine catalyzed by a D-amino acid oxidase [61], where the D-serine conversion was 90% with HA yield of 78% after the reaction at 25°C under bubbling of pure oxygen gas (10 mL) by adjusting pH = 7 using HCl aq. and NaOH aq.

In order to achieve the production of HA from glycerol using catalysts, it requires control of the catalytic reactivity to oxidize a terminal and a secondary OH group in glycerol without the oxidation of the other terminal OH group. To this end, PbO and Bi_2O_3 were introduced into CeO_2–ZrO_2, because the oxidation of secondary OH group can be facilitated owing to the geometric effect among glycerol, Pt, and Bi^{3+} or $Pb^{2+/4+}$ [62]. In addition, the replacement of the Ce^{4+} and Zr^{4+} sites for the lower-valent Bi^{3+} and Pb^{2+} ions generate the oxygen vacancies for oxide ion migration owing to the charge compensation mechanism, which can facilitate the oxygen supply ability. Moreover, since Pb has two kinds of valence states, Pb^{2+} and Pb^{4+}, further improvement of oxygen release and

storage abilities owing to the redox of $Pb^{2+/4+}$ is expected. The redox of $Pb^{2+/4+}$ and Bi^{3+} may improve the oxygen release and storage abilities. Therefore, novel catalysts of Pt/CeO_2–ZrO_2–Bi_2O_3–PbO/SBA-16 were prepared, and their catalytic activities for the glycerol oxidation were investigated under moderate conditions of the atmospheric open-air system and 30°C in a base-free solution.

3.2. Experimental Procedure

The required samples of 16wt%$Ce_{0.80(1-x-y)}Zr_{0.20(1-x-y)}Bi_yPb_xO_{2-\delta}$/SBA-16 (CZBi($y$)Pb($x$)/SBA) was synthesized by a co-precipitation method. Solutions of 1.0 mol·L^{-1} $Ce(NO_3)_3$, 0.10 mol·L^{-1} $ZrO(NO_3)_2$, 0.10 mol·L^{-1} $Pb(NO_3)_2$, and 0.50 mol·L^{-1} $Bi(NO_3)_3$, were prepared by dissolving $Ce(NO_3)_3·6H_2O$ (Kojundo, 99.9%), $ZrO(NO_3)_2·2H_2O$ (Kishida Chemical, ≥ 99.0%), and $Pb(NO_3)_2$ (FUJIFILM Wako Pure Chemical, 99.5%) in deionized water; and by dissolving Bi_2O_3 (Kishida Chemical, ≥ 99.9%) in 3 mol·L^{-1} nitric acid (prepared by diluting nitric acid (Kishida Chemical, 60%) with deionized water), respectively. The SBA-16 powder (0.4 g) was dispersed in the mixed solutions of 1.0 mol·L^{-1} $Ce(NO_3)_3$, 0.10 mol·L^{-1} $ZrO(NO_3)_2$, 0.50 mol·L^{-1} $Bi(NO_3)_3$, and 0.10 mol·L^{-1} $Pb(NO_3)_2$ in the stoichiometric ratio, and deionized water (30 mL) was added, followed by stirring for 30 min at room temperature. A solution of 5 vol% NH_3 (prepared by diluting aqueous NH_3 (Kishida Chemical, 28%) with deionized water) was added dropwise under vigorous stirring until the pH reached 11. After stirring for 12 h at room temperature, the precipitates were collected by suction filtration and dried at 80°C for 12 h, followed by calcination at 600°C for 1 h in atmospheric air.

Pt was loaded onto CZBi(y)Pb(x)/SBA was carried out using the impregnation procedure according to Chapter 1 to obtain 7wt%Pt/16wt%$Ce_{0.80(1-x-y)}Zr_{0.20(1-x-y)}Bi_yPb_xO_{2-\delta}$/SBA-16

(Pt/CZBi(*y*)Pb(*x*)/SBA).

XRD (SmartLab, Rigaku) was used to identify the crystal phase using Cu-Kα radiation (40 kV, 30 mA). The sample composition was examined using XRF (Supermini200, Rigaku). The BET specific surface area was measured at −196°C using N_2 gas (Micromeritics Tristar 3000, Shimadzu). TPR and OSC measurements were examined according to Chapter 1.The glycerol oxidation test and HPLC analysis were carried out at 30°C in the atmospheric air, as described in Chapter 1.

3.3. Results and Discussion

The measured compositions and surface area of Pt/CZBi(0.20)Pb(*x*)/SBA are listed in Table 3-1. The measured compositions of Pt/CZBi(0.20)Pb(*x*)/SBA were in good agreement with the feed values. The surface area decreased with increasing the Pb content (*x*).

Figure 3-1 shows XRD patterns of Pt/CZBi(0.20)Pb(*x*)/SBA. The broad peaks corresponding to the cubic fluorite-type structure were observed in addition to the peaks of the Pt metal and SBA-16. For all the catalysts, the crystallite sizes of Pt and the fluorite-type phase were almost the same ca. 5 and ca. 1 nm, respectively, irrespective of the Pb content. Although it is difficult to confirm the peak shift (Figure 3-1), the XRD measurements of CZBi(0.20)Pb(*x*)/SBA (Figure 3-2) demonstrated

Table 3-1. Measured composition and specific surface area of Pt/CZBi(0.20)Pb(*x*)/SBA

Catalyst	Measured composition	Specific surface area / $m^2 \cdot g^{-1}$
Pt/CZBi(0.20)/SBA	6.6wt%Pt/ 14.7wt%$Ce_{0.63}Zr_{0.18}Bi_{0.19}O_{2-\delta}$/SBA-16	298(2)
Pt/CZBi(0.20)Pb(0.05)/SBA	6.9wt%Pt/ 14.9wt%$Ce_{0.63}Zr_{0.14}Bi_{0.19}Pb_{0.04}O_{2-\delta}$/SBA-16	236(3)
Pt/CZBi(0.20)Pb(0.10)/SBA	6.3wt%Pt/ 15.1wt%$Ce_{0.54}Zr_{0.16}Bi_{0.18}Pb_{0.12}O_{2-\delta}$/SBA-16	220(1)

that the broad peaks of the fluorite-type structure were slightly shifted toward lower angles with increasing *x*, suggesting the replacement of the Ce^{4+} (0.111 nm [42]) and Zr^{4+} (0.098 nm [42]) sites for larger Pb^{2+} (0.143 nm [42]).

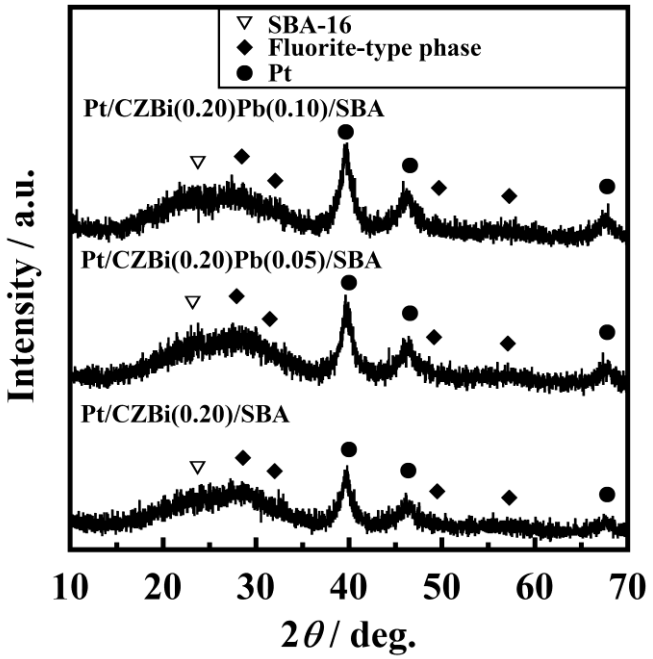

Figure 3-1. XRD patterns of Pt/CZBi(0.20)Pb(*x*)/SBA.

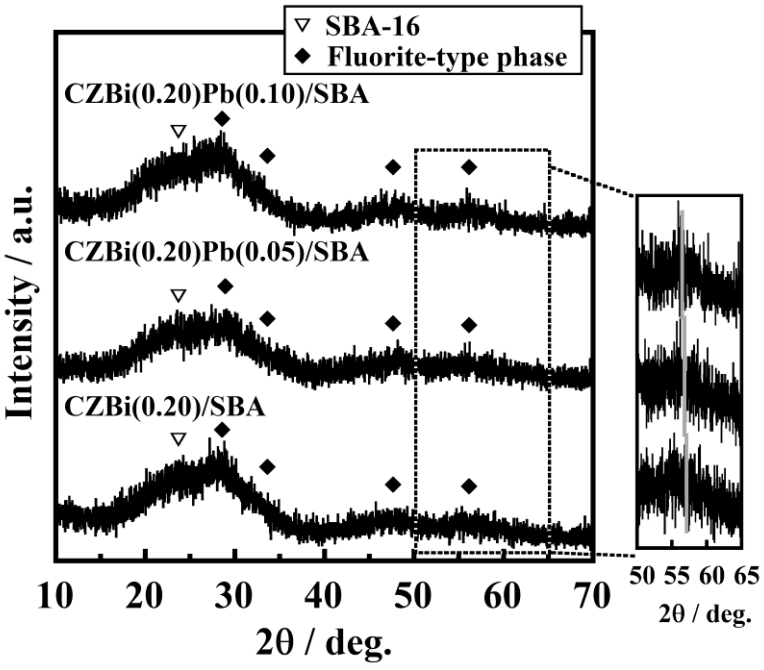

Figure 3-2. XRD patterns of CZBi(0.20)Pb(*x*)/SBA.

The effect of introducing $Pb^{2+/4+}$ on oxygen release and storage abilities was investigated using TPR measurements. Figure 3-3 displays the TPR profiles of CZBi(0.20)Pb(*x*)/SBA with the data of CZ/SBA, where the reduction peak top temperatures are summarized in Table 3-2. The introduction of Bi^{3+} and $Pb^{2+/4+}$ into CZ/SBA lowered the reduction temperature, and CZBi(0.20)Pb(0.05)/SBA showed the lowest peak temperature among CZBi(0.20)Pb(*x*)/SBA. In addition, OSC values were measured after the TPR analysis, and the results are also listed in Table 3-2. The OSC of CZBi(0.20)Pb(0.05)/SBA showed the highest value, followed by CZBi(0.20)Pb(0.10)/SBA, CZBi(0.20)/SBA, and CZ/SBA. Thus, CZBi(0.20)Pb(0.05)/SBA exhibited the highest oxygen release and storage abilities owing to the synergistic redox reaction between $Ce^{3+/4+}$ and $Pb^{2+/4+}$. Here, the decrease of the abilities for CZBi(0.20)Pb(0.10)/SBA might be caused by the decrease of the surface area.

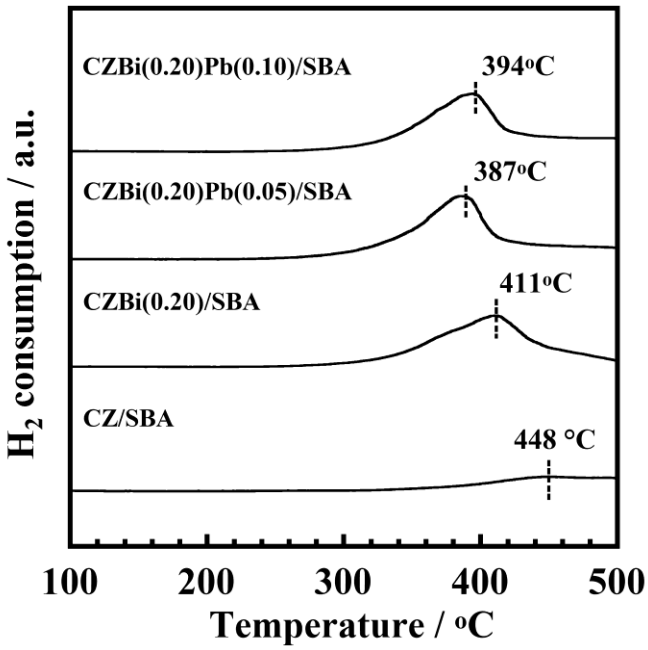

Figure 3-3. TPR profiles of CZBi(0.20)Pb(*x*)/SBA and CZ/SBA.

Table 3-2. Reduction peak temperature and OSC value of the CZBi(0.20)Pb(*x*)/SBA samples with the data of CZ/SBA

Sample	Reduction temperature / °C	OSC value / μmol $O_2 \cdot g^{-1}$
CZ/SBA	448	17
CZBi(0.20)/SBA	411	236
CZBi(0.20)Pb(0.05)/SBA	387	243
CZBi(0.20)Pb(0.10)/SBA	394	237

The glycerol oxidation test was carried out using Pt/CZBi(0.20)Pb(*x*)/SBA at 30°C for 4 h in atmospheric air, and the glycerol conversion and the HA yield are shown in Figure 3-4. For Pt/CZBi(0.20)Pb(0.05)/SBA, the glycerol conversion and the HA yield were remarkably enhanced compared to those of Pt/CZBi(0.20)/SBA. This behavior is attributed to the improvement of the oxygen release and storage abilities. Here, although HA is regarded as intermediate, which is easy to oxidize to chemically stable compounds such as OA, the moderate reaction condition enabled the

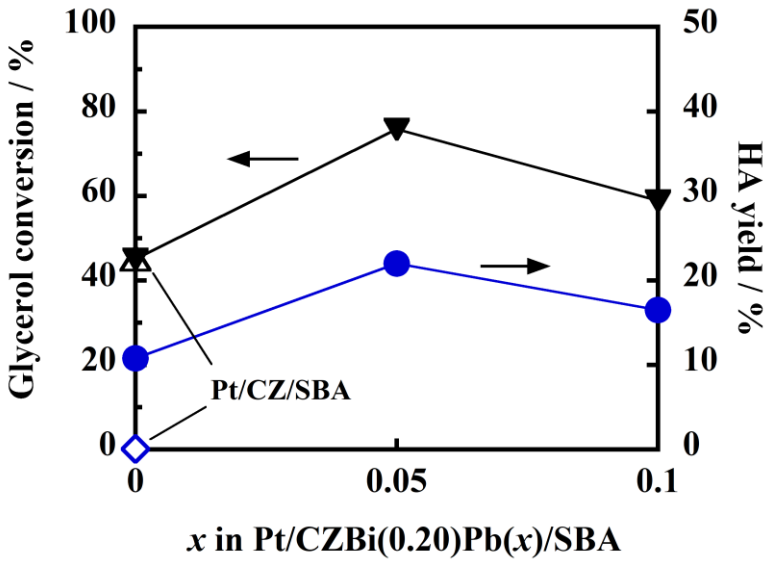

Figure 3-4. Glycerol conversion and HA yield of Pt/CZBi(0.20)Pb(*x*)/SBA and Pt/CZ/SBA at 30°C under the atmospheric air pressure for 4 h.

suppression of the further oxidation of HA, resulting in the high HA yield. In addition, because the HA yield for Pt/CZ/SBA was only 0.1%, the geometric effects of glycerol, Pt, and Bi^{3+} or $Pb^{2+/4+}$ facilitated the oxidation of the secondary OH group rather than the primary OH group. However, Pt/CZBi(0.20)Pb(0.10)/SBA showed a lower catalytic activity than Pt/CZBi(0.20)Pb(0.05)/SBA, likely due to the low surface area. Therefore, the optimum $Pb^{2+/4+}$ content (x) was determined to be 0.05.

Similarly, the Bi^{3+} content (y) was also optimized as presented in Figure 3-5. With introducing Bi content (y) into Pt/CZPb(0.05)/SBA, the glycerol conversion and the HA yield significantly increased up to y = 0.20. These results indicate that the Bi^{3+} introduction enhanced the glycerol oxidation ability and facilitated the oxidation of secondary OH group in glycerol. Consequently, the introduction of both Bi and Pb is important for the effective HA production, and the Pt/CZBi(0.20)Pb(0.05)/SBA catalyst exhibited the highest activity, in which the HA yield was 22.0%.

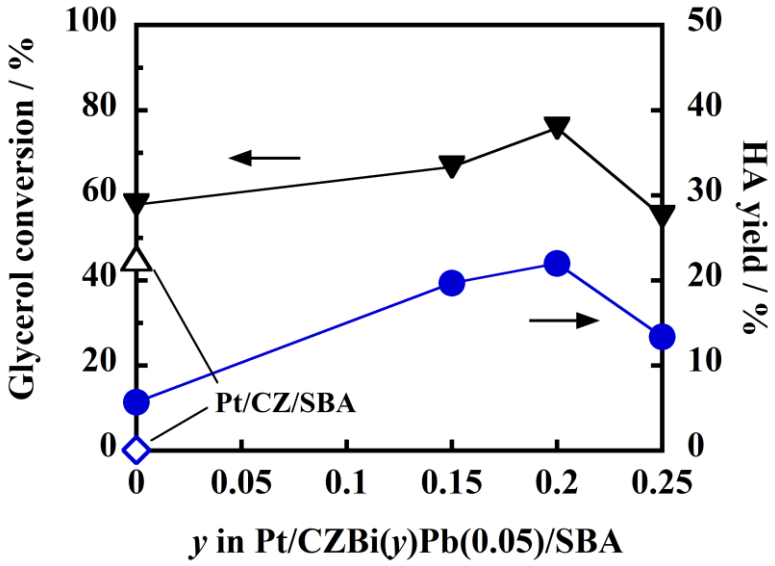

Figure 3-5. Glycerol conversion and HA yield of Pt/CZBi(y)Pb(0.05)/SBA and Pt/CZ/SBA at 30°C under the atmospheric air pressure for 4 h.

Figure 3-6 shows the glycerol oxidation activity as a function of reaction time over Pt/CZBi(0.20)Pb(0.05)/SBA at 30°C in atmospheric air, where TA and MA were not detected. DHA was predominantly produced, and its yield was increased with increasing the reaction time up to 6 h. The HA yield simultaneously increased, suggesting the conversion of DHA into HA (Figure G-1). Interestingly, even though GLOA and OA are chemically stable than HA, the yields of GLOA and OA, which are the further oxidation product of HA, remained low values (< 5%) compared to the HA yield. Thus, the moderate reaction conditions might suppress the further oxidation of HA to GLOA or OA. However, as the reaction time increased over 6 h, the HA yield decreased because of the decrease in the DHA yield and the further oxidation of HA. Therefore, the highest HA yield of 24.6% was obtained after the reaction for 6 h, where the glycerol conversion and the HA selectivity were 93.9% and 26.2%, respectively. Here, carbon mass balance maintained ca. 100% up to 6 h, while it decreased after 6 h. This behavior indicates the further oxidation to carbon dioxide and/or

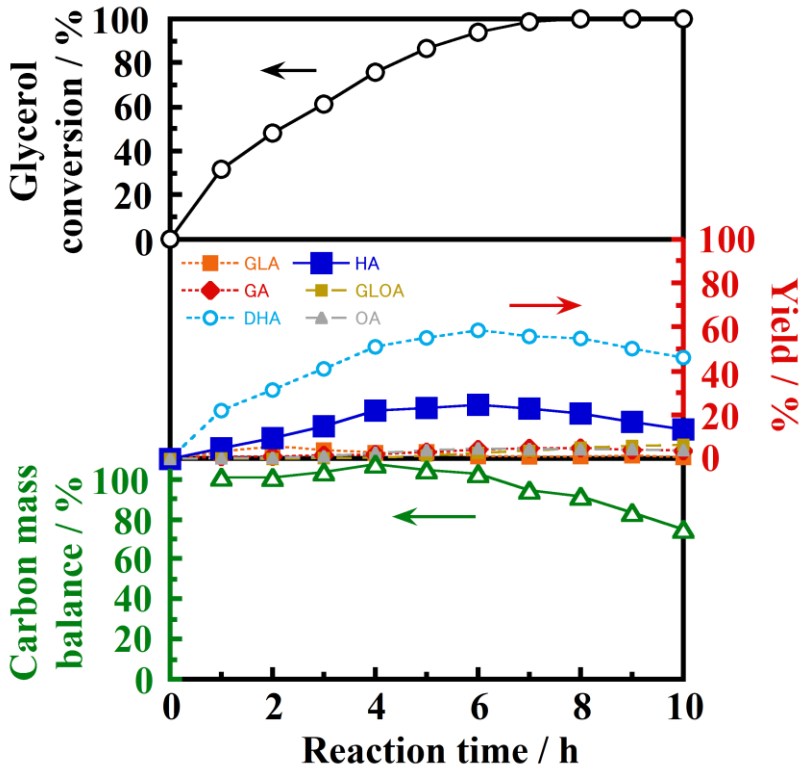

Figure 3-6. Glycerol conversion, the product yields, and carbon mass balance as a reaction time function for Pt/CZBi(0.20)Pb(0.05)/SBA at 30°C in the atmospheric air.

the adsorption of some products. This HA yield in the present thesis was higher than that of Au/graphite (22%) reported earlier after reaction at 30°C by applying 3 atm (pure O_2), with the addition of NaOH [10].

3.4. Conclusion

In this chapter, novel catalysts of Pt/CeO_2–ZrO_2–Bi_2O_3–PbO/SBA-16 were synthesized to convert glycerol into valuable hydroxypyruvic acid. Owing to the synergistic redox reaction between $Pb^{2+/4+}$ and $Ce^{3+/4+}$, CeO_2–ZrO_2–Bi_2O_3–PbO showed high oxygen release and storage abilities, which facilitated glycerol oxidation. Furthermore, the secondary OH group in glycerol was predominantly oxidized, likely due to the geometric effects of glycerol, Pt, and Bi^{3+} or $Pb^{2+/4+}$. Further oxidation of hydroxypyruvic acid was suppressed by employing moderate reaction conditions. Among the prepared catalysts, 7wt%Pt/16wt%$Ce_{0.60}Zr_{0.15}Bi_{0.20}Pb_{0.05}O_{2-\delta}$/SBA-16 exhibited the highest hydroxypyruvic acid yield of 24.6% after 6 h of reaction at 30°C in atmospheric air.

Summary

In the work of this doctoral thesis, in order to convert glycerol into value-added compounds of glyceraldehyde (GLA), glyceric acid (GA), and hydroxypyruvic acid (HA) under moderate condition (around room temperature in an atmospheric open-air system), novel catalysts based on CeO_2–ZrO_2 were developed. The main results and conclusions obtained in this study are summarized as follows:

Chapter 1

Pt/CeO_2–ZrO_2–Fe_2O_3/SBA-16 catalysts were synthesized to produce glyceraldehyde from glycerol effectively at around room temperature in an open air system. The introduction of Fe_2O_3 into the CeO_2–ZrO_2 lattice improved the oxygen release and storage abilities, which facilitated the oxidation of glycerol even under the moderate condition. Among the prepared catalysts, the 7wt%Pt/16wt%$Ce_{0.64}Zr_{0.16}Fe_{0.20}O_{2-\delta}$/SBA-16 catalyst exhibited the highest glyceraldehyde yield of 22.1% (glycerol conversion: 70.3%, glyceraldehyde selectivity: 31.4%) after the reaction for 4 h under the considerably moderate condition of 30°C in an open air atmosphere.

Chapter 2

For the effective production of glyceric acid from glycerol, the loading amount of CeO_2–ZrO_2–Fe_2O_3 was increased in the Pt/CeO_2–ZrO_2–Fe_2O_3/SBA-16 system. The increase of the CeO_2–ZrO_2–Fe_2O_3 loading amount led to the increase of oxygen release and storage abilities. The high amount of CeO_2–ZrO_2–Fe_2O_3 also caused the particle growth, which contributed to the lowering

of the number of acidic sites on the CeO_2–ZrO_2–Fe_2O_3 surface in the range over 16wt%. Due to the high oxygen release and storage abilities and the low acidity, the highest activity was obtained for 7wt%Pt/40wt%$Ce_{0.64}Zr_{0.16}Fe_{0.20}O_{2-\delta}$/SBA-16, which exhibited the high GA yield (68.2%) and selectivity (68.8%) with glycerol conversion (99.2%) even under moderate conditions after 10 h of reaction in an open-air system at 30°C.

Chapter 3

In order to produce intermediate of hydroxypyruvic acid from glycerol, novel catalysts of Pt/CeO_2–ZrO_2–Bi_2O_3–PbO/SBA-16 were synthesized. Owing to the synergistic redox reaction between $Pb^{2+/4+}$ and $Ce^{3+/4+}$, CeO_2–ZrO_2–Bi_2O_3–PbO showed high oxygen release and storage abilities, which facilitated glycerol oxidation. Furthermore, the secondary OH group in glycerol was predominantly oxidized, likely due to the geometric effects of glycerol, Pt, and Bi^{3+} or $Pb^{2+/4+}$. Moreover, further oxidation of HA was suppressed by employing moderate reaction conditions. Among the prepared catalysts, 7wt%Pt/16wt%$Ce_{0.60}Zr_{0.15}Bi_{0.20}Pb_{0.05}O_{2-\delta}$/SBA-16 exhibited the highest hydroxypyruvic acid yield of 24.6%, where the glycerol conversion and the HA selectivity were 93.9% and 26.2%, respectively, after 6 h of reaction at 30°C in atmospheric air.

References

[1] A. Salakkam, C. Webb, *Biochem. Eng. J.*, **137**, 358 (2018).

[2] J. Yu, F. Dappozze, J. M. Gomez, J. H. Carrillo, A. Marinas, P. Vernoux, A. Caravaca, C. Guillard, *Appl. Catal. B: Environ.*, **299**, 120616 (2021).

[3] R. Garcia, M. Besson, P. Gallezot, *Appl. Catal. A: Gen.*, **127**, 165 (1995).

[4] C. H. Zhou, H. Zhao, D. S. Tong, L. M. Wu, W. H. Yu, *Catal. Rev. Sci. Eng.*, **55**, 369 (2013).

[5] A. Corma, S. Iborra, A. Velty, *Chem. Rev.*, **107**, 2411 (2007).

[6] S. Bagheri, N. M. Julkapli, W. A. Yehye, *Renew. Sust. Energ. Rev.*, **41**, 113 (2015).

[7] T. G. Vo, P. Y. Ho, C. Y. Chiang, *Appl. Catal. B: Environ.*, **300**, 120723 (2022).

[8] L. Yang, X. Li, P. Chen, Z. Hou, *Chin. J. Catal.*, **40**, 1020 (2019).

[9] S. Carrettin, P. McMorn, P. Johnston, K. Griffin, G. J. Hutchings, *Chem. Commun.*, **7**, 696 (2002).

[10] N. Dimitratos, F. Porta, L. Prati, *Appl. Catal. A: Gen.*, **291**, 210 (2005).

[11] R. Garcia, M. Besson, P. Gallezot, *Appl. Catal. A: Gen.*, **127**, 165 (1995).

[12] M. Zhang, R. Nie, L. Wang, J. Shi, W. Dua, Z. Hou, *Catal. Commun.*, **59**, 5 (2015).

[13] X. Zhang, D. Zhou, X. Wang, J. Zhou, J. Li, M. Zhang, Y. Shen, H. Chu, Y. Qu, *ACS Catal.*, **10**, 3832 (2020).

[14] S. Chen, P. Qi, J. Chen, Y. Yuan, *RSC Adv.*, **5**, 31566 (2015).

[15] J. Lei, X. Duan, G. Qian, X. Zhou, D. Chen, *Ind. Eng. Chem. Res.*, **53**, 16309 (2014).

[16] F. F. Wang, S. Shao, C. L. Liu, C. L. Xu, R. Z. Yang, W. S. Dong, *Chem. Eng. J.*, **264**, 336 (2015).

[17] R. Garcia, M. Besson, P. Gallezot, *Appl. Catal. A: Gen.*, **127**, 165 (1995).

[18] L. Dan, C. Shiyu, G. Jing, W. Junhua, C. Ping, H. Zhaoyin, *Chin. J. Catal.*, **32**, 1831 (2011).

[19] D. Liang, J. Gao, J. Wang, P. Chen, Y. Wei, Z. Hou, *Catal. Commun.*, **12**, 1059 (2011).

[20] M. Zhanga, J. Shia, W. Ningb, Z. Hou, *Catal. Today*, **298**, 234 (2017).

[21] H. Tan, O. E. Tall, Z. Liu, N. Wei, T. Yapici, T. Zhan, M. N. Hedhill, Y. Han, *ChemCatChem*, **8**, 1699 (2016).

[22] D. Liang, J. Gao, H. Sun, P. Chen, Z. Hou, X. Zheng, *Appl. Catal. B: Environ.*, **106**, 423 (2011).

[23] H. F. Wang, X. Q. Gong, Y. L. Guo, Y. Guo, G. Z. Lu, P. Hu, *J. Phys. Chem. C*, **113**, 10229 (2009).

[24] T. Suzuki, A. Morikawa, A. Suda, H. Sobukawa, M. Sugiura, T. Kanazawa, J. Suzuki, T. Takada, *R&D Rev. Toyota CRDL*, **37**, 28 (2002).

[25] R. Breslow, V. Ramalingam, C. Appayee, *Orig. Life Evol. Biosph.*, **43**, 323 (2013).

[26] R. Breslow1, Z. L. Cheng, *Proc. Natl. Acad. Sci. U.S.A.*, **107**, 5723 (2010).

[27] M. Yokota, M. Sekita, Y. Okano, H. Masaki, M. Takeuchi, Y. Tokudome. *Ann Dermatol.*, **29**, 508 (2017).

[28] P. Ulrich, A. Cerami, *Recent Prog. Horm. Res.*, **56**, 1 (2001).

[29] R. Nagai, Y. Fujiwara, K. Mera, K. Motomura, Y. Iwao, K. Tsurushima, M. Nagai, K. Takeo, M. Yoshitomi, M. Otagiri, T. Ikeda, *Ann. N.Y. Acad. Sci.*, **1126**, 38 (2008).

[30] L. C. Maillard, *C. R. Acad. Sci.*, **154**, 66 (1912).

[31] A. Cerami, H. Vlassara, M. Brownlee, *Sci. Am.*, **256**, 90 (1987).

[32] S. Miyata, V. Monnir, *J. Clin. Invest.*, **89**, 1102 (1992).

[33] T. Niwa, T. Katsuzaki, S. Miyazaki, *J. Clin. Invest.*, **99**, 1272 (1997).

[34] H. Yonekura, Y. Yamamoto, S. Sakurai, T. Watanabe, H. Yamamoto, *J. Pharmacol. Sci.*, **97**, 305 (2005).

[35] V. P. Reddy, M. E. Obrenovich, C. S. Atwood, G. Perry, M. A. Smith, *Neurotox. Res.*, **4**, 191 (2002).

[36] H. Sueki, S. Nozaki, R. Fujisawa, K. Aoki, Y. Kuroiwa, *J. Dermatol.*, **16**, 103 (1989).

[37] K. M. Reiser, *Pros. Soc. Exp. Biol. Med.*, **28**, 23 (1998).

[38] V. M. Monnier, O. Bautista, D. Kenny, D. R. Sell, J. Fogarty, W. Dahms, P. A. Cleary, J. Lachin, S. Genuth, *Diabetes*, **48**, 870 (1999).

[39] G. Hein, *Clin. Chim. Acta*, **371**, 32 (2006).

[40] M. Jeong, N. Nunotani, N. Imanaka, *Bull. Chem. Soc. Jpn.*, **91**, 158 (2018).

[41] H. Yotou, T. Okamoto, M. Ito, T. Sekino, S. I. Tanaka, *Appl. Catal. A: Gen.*, **458**, 137 (2013).

[42] R. D. Shannon, *Acta Crystallogr. Sect. A*, **32**, 751 (1976).

[43] A. R. Supandi, N. Nunotani, N. Imanaka, *J. Environ. Chem. Eng.*, **5**, 3999 (2017).

[44] M. A. L. Rochaa, G. D. Ángela, G. T. Torresb, A. Cervantesa, A. Vázqueza, A. Arrietaa, J. N. Beltramini, *Catal. Today*, **250**, 145 (2015).

[45] S. Sato, *J. Oleo Sci.*, **70**, 289 (2021).

[46] K. Lešová, M. Šturdíková, B. Proksa, M. Pigoš, T. Liptaj, *Folia Microbiol.*, **46**, 21 (2001).

[47] C.J. P. Eriksson, T. P. S. Saarenmaa, I. L. Bykova, P. U. Heino, *Metab. Clin. Exp.*, **56**, 895 (2007).

[48] H. Habe, S. Sato, T. Fukuoka, D. Kitamoto, K. Sakaki, *J. Oleo Sci.*, **60**, 585 (2011).

[49] S. Sato, D. Kitamoto, H. Habe, *Biosci. Biotechnol. Biochem.*, **78**, 1183 (2014).

[50] H. Habe, Y. Shimada, T. Yakushi, H. Hattori, Y. Ano, T. Fukuoka, D. Kitamoto, M. Itagaki, K. Watanabe, H. Yanagishita, K. Matsushita, K. Sakaki, *Appl. Environ. Microbiol.*, **75**, 7760 (2009).

[51] X. Liu, P. R. Jensen, M. Workman, *Biores. Technol.*, **104**, 579 (2012).

[52] H. Habe, Y. Shimada, T. Fukuoka, D. Kitamoto, M. Itagaki, K. Watanabe, H. Yanagishita, K. Sakaki, *Biosci. Biotechnol. Biochem.*, **73**, 1799 (2009).

[53] S. Sato, N. Morita, D. Kitamoto, T. Yakushi, K. Matsushita, H. Habe, *AMB Express*, **3**, 20 (2013).

[54] S. Gerstenbruch, H. Wulf, N. Mußmann, T. Connell, K. H. Maurer, U. T. Bornscheuer, *Appl. Microbiol. Biotechnol.*, **96**, 1243 (2012).

[55] Y. H. Wang, W. G. Gao, H. Wang, Y. E. Zheng, W. Na, K. Z. Li, *RSC Adv.*, **7**, 8709 (2017).

[56] T. Désaunay, G. Bonura, V. Chiodo, S. Freni, J. P. Couzinié, J. Bourgon, A. Ringuedé, F. Labat, C. Adamo, M. Cassir, *J. Catal.*, **297**, 193 (2013).

[57] M. Lykaki, S. Stefa, S. A. C. Carabineiro, P. K. Pandis, V. N. Stathopoulos, M. Konsolakis, *Catalysts*, **9**, 371 (2019).

[58] A. R. Supandi, N. Nunotani, N. Imanaka, *J. Asian Ceram. Soc.*, **8**, 745 (2020).

[59] A. Abbadi, H. van Bekkum, *Appl. Catal. A: Gen.*, **148**, 113 (1996).

[60] L. Hecquet, C. Demuynck, G. Schneider, J. Bolte, *J. Mol. Catal. B: Enzym.*, **11**, 771 (2001).

[61] M. Lenfant, F. Bruna, M. Lorillière, N. Ocal, W. D. Fessner, L. Pollegioni, F. Charmantray, L. Hecquet, *Adv. Synth. Catal.*, **361**, 2550 (2019).

[62] C. H. Zhou, J. N. Beltramini, Y. X. Fana, G. Q. Lu, *Chem. Soc. Rev.*, **37**, 527 (2008).

Acknowledgments

The author would like to express his heartfelt gratitude to Professor Dr. Nobuhito Imanaka, Department of Applied Chemistry, Graduate School of Engineering, Osaka University, for his continuous guidance, many invaluable suggestions, and science encouragement throughout the work. The author is very grateful to Dr. Naoyoshi Nunotani, Department of Applied Chemistry, Graduate School of Engineering, Osaka University, for his continuous guidance and stimulating discussions for carrying out this work. The author is also indebted to Dr. Shinji Tamura, Department of Applied Chemistry, Graduate School of Engineering, Osaka University, for his helpful suggestions and apposite advice.

The author is deeply grateful to Professor Dr. Hidehiro Sakurai, Department of Applied Chemistry, Graduate School of Engineering, Osaka University, and Professor Dr. Takahiro Kozawa, the Institute of Scientific and Industrial Research (Department of Applied Chemistry, Graduate School of Engineering), Osaka University, for reviewing this thesis and giving their valuable comments.

I wish to thank Dr. Hirokazu Izumi (Hyogo Prefectural Institute of Technology) for his assistance during XPS measurement. I also thank Dr. Takao Sakata and Prof. Dr. Jun Yamasaki (Research Center for Ultra-High Voltage Electron Microscopy, Osaka University) for helping us with the TEM observation.

Special thanks should be given to author's co-workers, Mr. Kenji Matsuo, Mr. Masanari Takashima, Dr. Abdul Rohman Supandi, Mr. Kenjiro Kakihana, Mr. Kunimitsu Morita, Mr. Won-Joon Lee, Mr. Hiroaki Shirai, Mr. Momai Mizuki, Dr. Pil-Gyu Choi, Dr. Min-Chan Jeong, Dr. Chang-Min Cho, Dr. Won-Rak Lee, Dr. Muhammad Radzi Iqbal Bin Misran, Ms. Marina Taira, Mr. Yang Li, Ms. Li Zhouwei, Mr. Hu Dongrun for their helpful assistance and support in the course of

this work, and the other members of the research group under direction of Professor Dr. Nobuhito Imanaka, Osaka University.

The author would like to thank to Professor Dr. Dong-Sik Bae, Dr. Jeong-Hun Son, and Professor Dr. Yeon-Gil Jung of Changwon National University, Dr. Sun-Woog Kim of Korea Institute of Ceramic Engineering and Technology, Dr. Byung-Seo Bae of Yeongwol Industrial Promotion Agency, and Dr. Do-Yoon Kim of Korea Shipbuilding & Offshore Engineering, Advanced Research Center in South Korea for their helpful comments and encouragement.

The Otsuka Toshimi Scholarship, Japan is also acknowledged for financial support during the author's study.

Finally, the author would like to extend deep gratitude to his parents, Mr. Gyeong-Sik Choi and Ms. Gyeong-Ja Noh, his sister Yes-Seul Choi, and all the member of his family for their encouragement, continuous understanding, and perpetual supports.